Characterizing and evaluating the bonding between TiO_2 nanotubes and dental porcelain

BY

HIMANI NADGAUDA

B.S., University of California, Berkeley, 2013

THESIS

Submitted as partial fulfillment of the requirements for the degree of Master of Science in Chemical Engineering in the Graduate College of the University of Illinois at Chicago, 2015

Chicago, Illinois

Defense Committee

Professor Christos Takoudis, Chair and Advisor
Professor Cortino Sukotjo, College of Dentistry
Professor Tolou Shokuhfar, Bioengineering
Professor Vikas Berry
Professor Mathew Mathew, Rush University Medical Center

Dedication

I dedicate this work to my family and friends, without whom my accomplishments would not have been possible. I especially thank my parents and sister. Their constant, unwavering, and patient support has held me up throughout my academic studies and thesis work. I am forever grateful to them.

Acknowledgements

This work was carried out at University of Illinois at Chicago (UIC) and Rush University. I wish to thank the UIC College of Dentistry for making it financially possible to complete this study.

I gratefully thank my advisor, Professor Christos Takoudis (UIC Chemical Engineering and Bioengineering), for guiding me to think analytically, improving my writing to be precise and scientifically accurate, and in providing constant encouragement and support. I also wish to thank my other advisor, Professor Cortino Sukotjo (UIC College of Dentistry), for inviting me to partake into an important research project, for the discussions throughout the stages of completing this study, and for providing me with broad access to the dental facilities and equipment.

To Professor Tolou Shokuhfar (UIC Bioengineering) I owe my sincere thanks for sharing her insight regarding titanium dioxide nanotubes and for allowing me to use her lab space, which was essential to my completing this study.

I gratefully acknowledge Dr. Ryan Matthews for his invaluable help with the clinical aspects and statistical analysis of this project. His positive attitude and cheerful disposition made working on this study an enjoyable experience.

I would also like to thank Eric Schmidt (UIC Machine Shop) for his assistance with the mechanical testing portion of this work, Professor Ana Bedran-Russo (UIC College of Dentistry) for allowing me to use her lab space, and Dr. Marlos Viana (UIC College of Medicine) for sharing his expertise on statistics.

Acknowledgements (continued)

I would also like to acknowledge my academic colleagues Sweetu Patel, Maria Runa, and Ariene Leme for their assistance in surface characterization and advice throughout my research process. I am deeply grateful for the input provided by the faculty and student members comprising the Institute of Biomaterials, Tribocorrosion and Nanomedicine (IBTN).

Finally, I would like to thank the UIC Department of Chemical Engineering and UIC Office of Technology Management for tuition funding which made it possible for me to support myself while completing this work.

Table of Contents

Table of Contents (continued)

List of Figures

List of Figures (continued)

List of Figures (continued)

List of Figures (continued)

List of Tables

List of Abbreviations

ALD	Atomic layer deposition
CAD/CAM	Computer-aided design and computer-aided manufacturing
CTE	Coefficient of thermal expansion
CVD	Chemical vapor deposition
EDS	Energy dispersive X-ray spectrometry
FESEM	Field emission electron microscopy
PFM	Porcelain fused to metal restoration
PVD	Physical vapor deposition
T_g	Glass-transition temperature
TNT	Titanium dioxide nanotube
XPS	X-ray photoelectron spectroscopy
XRD	X-Ray diffraction
YSZ	Yttria-stabilized zirconia

Summary

The following body of work aims to strengthen the bonding between titanium and dental porcelain through achieving mechanical interlocking at the interface. Electrochemical anodization was used to create titanium dioxide nanotubes on the titanium surface in hopes that when porcelain was added on top of the metal, the resulting increased surface area would lead to stronger bond strength between the two materials. Titanium samples were electrochemically anodized at 60 V for 0, 1, 5, 15, and 30 minutes so as to grow nanotubes of different lengths. Dental porcelain was added onto the titanium and the metal-ceramic samples were subsequently fired in a furnace. The bond strength of these samples was evaluated using the 3-point bending method, following ISO 9693 standards.

Results showed that the highest average debonding strength values for both the grade 2 and grade 5 samples occurred for the 0 min anodization time (grade 2: 16.1±2.4 MPa, grade 5: 16.9±3.0 MPa) and 5 min anodization time groups (grade 2: 15.8±2.5 MPa, grade 5: 18.5±2.9 MPa). It was found that the grade 2 and 5 samples without nanotubes adhered to the ceramic equally well as the grade 2 and 5 samples that had been anodized for 5 min. These two groups were able to withstand the highest average load during the 3-point bending test compared to the grade 2 and 5 samples at the other anodization times used (1, 15, and 30 min). The ANOVA analysis of the results revealed that the debonding strength, τ_b, of the grade 5 metal-ceramic samples was greater than that of grade 2 metal-ceramic samples. Student t-test results showed that the mean τ_b of grade 2 metal-ceramic samples anodized for 1 and 15 min and grade 5 metal-ceramic samples anodized for 1 min was

significantly lower than the un-anodized metal-ceramic samples. Rutile formation may have occurred on the titanium samples during the porcelain firing process due to the exposure to high temperatures in the dental furnace. This may have caused collapse of some of the TNTs on the metal-ceramic samples. For every metal-ceramic sample, the break during the 3-point bending test occurred in a jagged fashion; the break appeared to be both a substrate failure and cohesive failure. These findings suggested that there is a need for further research on developing a coating that can withstand the high temperatures in the dental furnace, lead to successful wetting of porcelain on the metal surface, and successfully achieve stronger bonding between the titanium and dental porcelain during the firing process.

Chapter 1

Introduction

1.1 Porcelain fused to metal restorations

A porcelain fused to metal restoration (PFM) is a combination of an esthetic porcelain veneering material and a metal substructure, called a coping. PFMs are used to protect weak teeth from breaking, restore broken teeth, and cover up misshapen teeth and dental implants. They have a 10-year success rate of about 95%.

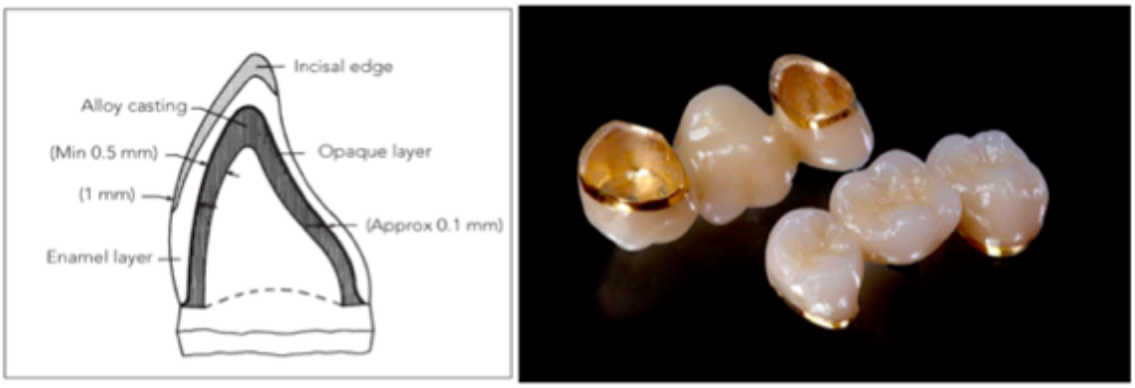

Figure 1.1 Cross sectional view of a PFM structure (O'Brien, 1997) (left), PFM with a gold coping ("Porcelain Fused to Metal « A-1 Dental Lab," n.d.) (right).

In PFMs, the porcelain provides the esthetic veneer and the metal provides the strength (Shillingburg, Jacobi, & Brackett, 1987). The porcelain portion of the PFM is usually composed of two ceramic layers; the first being the opaque layer, which masks the darkness of the underlying oxidized metal, and the second being the dentin (also known as the enamel) layer, which produces a natural tooth-like appearance (Powers, 2012) (Shillingburg et al., 1987). The porcelain portion of PFMs is usually 1 mm thick. The thickness of the metal coping portion of PFMs depends on the metal used. If a more malleable metal is used, the thickness is 0.3-0.5 mm and if a harder metal is used, the thickness is around 0.2 mm (Shillingburg et al., 1987).

Porcelain is added as a paste onto the metal substructure, and the metal ceramic combination is fired in a furnace. During the firing, an oxide forms on the metal. The atoms from the metal and porcelain diffuse into this oxide layer, thus forming a chemical bond (O'Brien, 1997) (Powers, 2012). Silicates can form from the reaction of metal oxides with the silicon in the porcelain (Darvell, 2009).

When PFMs fail, it is due to adhesive failure between porcelain and metal or cohesive failure within ceramic near the metal-ceramic interface (Powers, 2012). A cohesive failure translates to a failure occurring in the porcelain. An adhesive failure entails a break occurring at the interface between the porcelain and the metal oxide layer.

Historically, gold has been the preferred metal of choice for dental restorations. This is because of its excellent bond strength to dental porcelains (Lim, Kim, Lee, & Park, 2011). However, the price of gold has steadily increased to the point where cheaper metals are sought after for dental restorations. Base metals have been evaluated as replacements for gold (Yilmaz & Dinçer, 1999) (Akova, Ucar, Tukay, Balkaya, & Brantley, 2008) (de Melo, Travassos, & Neisser, 2005). However, base metal alloys have negative attributes when used in dental restorations such as poor biocompatibility, low corrosion resistance, and the tendency to discolor porcelain (Yilmaz & Dinçer, 1999) (Powers, 2012). As a result, titanium has become the next coping metal of choice for the reasons detailed in section *1.3*.

1.2 Porcelain

1.2.1 Porcelain Properties

Porcelain is a white and translucent ceramic that has similar appearance to teeth. It is also durable and biocompatible (O'Brien, 1997). For these reasons, it is the ideal candidate for being used as the outer veneer in PFMs.

Dental porcelains are classified according to their fusion temperature. Titanium has a tendency to form flaky and nonadherent oxides when exposed to high temperatures. Due to this, low-fusing porcelains are added on top of titanium metals. These porcelains fuse around 660°C to 1,066°C.

Dental porcelains are mostly composed of leucite, which has the chemical formula of potassium aluminum tectosilicate ($K(AlSi_2O_6)$). Dental porcelains also contain silica (SiO_2), alumina (Al_2O_3), sodium oxide (Na_2O), potassium oxide (K_2O), and feldspar ($K_2O{\cdot}Al_2O_3{\cdot}6SiO_2$) (Powers, 2012). Feldspar melts at 1150°C, and forms leucite which is $K(AlSi_2O_6)$ or $K_2O{\cdot}Al_2O_3{\cdot}4SiO_2$. The opaque layer of porcelain, often closest to the metal, is composed of TiO_2, ZrO_2, SnO_2, and CeO_2 (Powers, 2012)(O'Brien, 1997).

1.2.2 Porcelain Manufacturing

Dental porcelain is manufactured by a multi-step process (Powers, 2012). Raw materials such as feldspar ($K_2O{\cdot}Al_2O_3{\cdot}6SiO_2$), silica ($SiO_2$), alumina ($Al_2O_3$), sodium oxide ($Na_2O$), and potassium oxide ($K_2O$) are mixed together and heated to around 1200°C at which point a glassy phase is formed. The mixture is then quenched in water and the glassy phase shatters into small fragments. The fragments are ball-milled to obtain a homogenous particle size. The particle sizes of dental porcelain can range from <1 to >60 μm. The majority of dental porcelain particles are 10-20 μm (Rasmussen, Ngaji-Okumu, Boenke, & O'Brien, 1997). Colors are added to the porcelain mixture by including ceramic compounds such as iron oxides.

1.2.3 Porcelain Firing Process

As mentioned in the previous section, porcelain powder is mixed with a liquid and subsequently applied to the metal using a brush. Each layer of porcelain is added one by

one. After each layer is added onto the metal, a vibrator and adsorbent tissue is used to remove water. This increases both the strength and density of the burgeoning ceramic structure. As each layer of the PFM is built up, the layers are sintered one-by-one in a dental furnace.

There is often a vacuum environment in the dental furnace to minimize excessive oxidation of the metal. During the firing process, porcelain softens, its viscosity decreases, and it wets the metal surface. Through this way, any residual pores are closed and interlocking between porcelain and the metal occurs (Powers, 2012) (Bergmann & Stumpf, 2013).

1.3 Titanium

1.3.1 Titanium Properties

Titanium and titanium alloys have many positive attributes, which make them attractive for use in dental restorations. They have excellent corrosion resistance (Lim et al., 2011) (Khung & Suansuwan, 2013), high strength (Lim et al., 2011) (S. Park et al., 2009), high microhardness (Lim et al., 2011) (S. Park et al., 2009), are biocompatible (Suansuwan & Swain, 2003) (Khung & Suansuwan, 2013), and are of low cost (Adachi, Mackert, Parry, & Fairhurst, 1990).

The corrosion resistance and biocompatibility of titanium at room, oral, and body temperatures are attributed to the formation of a stable oxide film with a thickness of less than 1 nm. If this film is scratched or abraded, the involved area repassivates instantly (Noort, 1987). However, at high temperatures, the oxide film is not protective because it thickens and becomes nonadherent.

Grade 2 (also known as commercially pure) titanium is an alloy of mostly titanium and a minimal amount of oxygen (Noort, 1987). Grade 5 (also referred to as Ti6Al4V) titanium is an alloy with the chemical composition of 6% aluminum, 4% vanadium, a minimal amount of iron and oxygen, with the rest being titanium. As the oxygen or iron content in titanium increases, its strength increases but ductility decreases. Thus, grade 2 titanium has lower strength compared to grade 5 titanium. However, both grades are used in dental implants.

1.3.2 Titanium Manufacturing

Titanium can be processed through casting or with computer-aided design and computer-aided manufacturing (CAD/CAM) technology. Casting of titanium is problematic due to titanium's excessively reactive nature at high temperatures. The melting point of titanium is high (1,700°C) and therefore the titanium casting temperature is around 2000°C. Titanium tends to react with the investment material it is cast into and forms a hard and brittle surface layer (O'Brien, 1997). Thus CAD/CAM technology is now commonly used to form titanium copings from prefabricated stock due to the prevention of such a layer (Khung & Suansuwan, 2013).

1.4 Problems with bonding titanium to dental porcelain

1.4.1 Coefficient of Thermal Expansion

There are setbacks that prevent titanium from being the ideal metal in PFMs. The CTE of the veneering porcelain should be lower than that of the underlying metal to ensure that the ceramic is in a compressed state after cooling. This establishes ceramic's ability to have superior resistance to crack propagation. When porcelain is under compression it is less sensitive to tensile stresses induced by mechanical loading (Powers, 2012) (Darvell,

2009). Titanium has a lower coefficient of thermal expansion (CTE) compared to other PFM alloys. It is 9.4×10^{-6}/°C versus 13 to 16×10^{-6}/°C (Okabe, 1998) (Khung & Suansuwan, 2013). This is the reason why low fusing porcelains with CTE values of $9x10^{-6}$/°C are used with titanium. However, the difference between the CTEs of low fusing porcelains and titanium do not differ by a great amount.

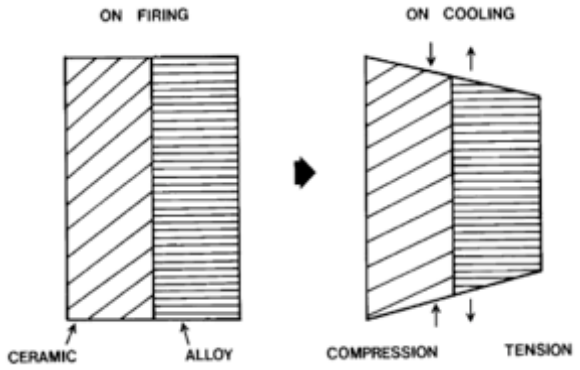

Figure 1.2 Metal-ceramic sample during firing (left) and upon cooling (right) (Darvell, 2009).

1.4.2 Nonadherent Oxide Formation at the Interface Between Titanium and Porcelain

The nonadherent oxide layer that forms on titanium from the high heat exposure during the porcelain firing process is one of the factors for why titanium metal is not as stable in PFMs as the nonreactive gold (S. Park et al., 2009). During the porcelain firing process, both the titanium and porcelain are exposed to high heat. However, the Gibbs free energies of the various forms of titanium dioxide are much greater (negative) than the Gibbs free energies created by the formation of oxide phases in porcelain (1999 R. Wang), leading to the formation of titanium oxides at the interface of PFMs. Oxygen is highly soluble in solid state titanium and even more so in the molten state titanium takes in the dental furnace. Thermodynamically, the equilibrium reaction between titanium and oxygen corresponds to a range of 10^{-30} to 10^{-42} atm O_2 partial pressure between 700°C and 1000°C. Mechanical vacuums commonly used for conventional dental furnaces have a vacuum level

of only around 10^{-2} to 10^{-5} atm. Thus the vacuum atmosphere of dental furnaces isn't sufficient to prevent titanium oxidation during dental porcelain (1999 R. Wang).

Oxidation of any material is based by the diffusion of oxygen. The oxide thickness can be expressed like this according to a previous study (Diserens, Patscheider, & Lévy, 1999).:

$$d_{oxide} = \sqrt{2Dt} \quad \text{.....Eqn. 1.1}$$

where t is the oxidation time, and D is the diffusion coefficient of oxygen in titanium dioxide. Since oxidation is a thermally activated process, D can be described by the Arrhenius law:

$$D = D_o e^{-\frac{E_a}{RT}} \quad \text{.....Eqn. 1.2}$$

where E_a is the thermal activation energy associated with the oxidation process, D_0 is the pre-exponential factor, R is the gas constant, and T is the temperature. Oxidation of titanium occurs through the inward lattice diffusion of oxygen, with new oxide forming at the oxide-metal interface (Adachi et al., 1990). The failure of the titanium dioxide to form a protective scale at high temperatures is thought to be due to stress build-up in the inwardly growing oxide scale. This stress buildup exceeds the strength of the scale when the oxide layer becomes about 1 μm thick, causing the scale to fracture and expose new metal to the oxidizing atmosphere (Adachi et al., 1990).

A compact, adherent oxide scale is formed below 800°C during short oxidation times in a dental furnace, but a poorly adherent, porous scale is formed above 800°C and during longer oxidation times (Adachi et al., 1990). X-Ray diffraction (XRD) analysis revealed that the oxide layers formed on both the grade 2 and grade 5 titanium specimens during high temperature (1000°C) oxidation treatment were composed of the rutile form of TiO_2.

1.5 Previous studies to improve bonding between metals and dental porcelain

1.5.1 Chemical Coatings of Titanium

Various pure metals and ceramics have been used to coat titanium surfaces before the application of porcelain in order to prevent excessive titanium oxidation during the porcelain firing process. These coatings serve as barriers to oxygen diffusion into the titanium. A myriad of tests were done to test if the coated titanium had a stronger bond to the dental porcelain compared to the uncoated titanium.

Gold has been used to coat titanium through a sputtering technique (S. Park et al., 2009) (Khung & Suansuwan, 2013) (Lim et al., 2011). The gold-coated titanium has displayed higher bonding strength than uncoated titanium and even the titanium coated with different materials. Zirconium silicon nitride (ZrSiN) coatings with different amounts of silicon have been tested on titanium (T. Zhang et al., 2014). The coating with the highest atomic percentage of silicon (18 at. %) has displayed the strongest bond with porcelain in this case. Titanium nitride (TiN) (S. Park et al., 2009), Calcium stabilized zirconia (ZrO_2-CaO) and nickel-aluminum-molybdenum + calcium stabilized zirconia (Ni-Al-Mo+ ZrO_2-CaO) (Marcelli et al., 2014), and silicon nitride (Si_3N_4) (Wang, Welsch, & Monteiro, 1999) are among some other coatings that have successfully increased the bonding between titanium and porcelain. These are a purely chemical means to increase the bonding between the metal and ceramic. Since porcelain is a molten glass during the firing procedure, it is chemically dissimilar to the underlying metal. As a result, no true adhesion can be obtained solely from chemical van der Waals forces. Mechanical retention through roughening the metal surface by abrasion or etching can be used to obtain interlocking between the metal and ceramic (Darvell, 2009).

1.5.2 Mechanical Retention through Roughening Techniques

Mechanical means can also be used to increase the bonding between titanium and dental porcelain. When a fracture occurs between the porcelain and the roughened titanium metal, the path of the fracture deviates rather than taking a straight path. This increases the fracture surface area and the total energy required for failure. Roughening of metals on which porcelain is to be added is advised because it allows for the small scale interlocking with the ceramic (Darvell, 2009) (O'Brien, 1997). Sandblasting with micron-size alumina particles and acid etching of titanium are methods to increase the roughness of titanium on the micron and nano-scale.

A previous study has been done to evaluate the effects of a nanoporous film on the bonding strength between grade 2 titanium and porcelain (Guo et al., 2013). In that work, the nanoporous film was created by electrochemical anodization. The anodized samples have 200 nm diameter pores. Porcelain is applied on the anodized samples and the finished samples are subjected to a 3-point bending test. All conditions are set to ISO 9693 standards. The investigators have concluded that the group of anodized samples show a 7% improvement in bonding strength compared to the control group due to the mechanical interlocking effect.

Mechanical interlocking is one of the factors that come into play for porcelain and metal bonding. In previous research, the increased surface roughness of titanium led to additional contact area and mechanical interlocking between titanium and porcelain. This increased the bonding between the two materials (Litong Guo et al., 2010). Since nanotubes have more surface area than nanopores, in this study, nanotubes are grown on both commercially pure (grade 2) titanium and Ti6Al4V (grade 5) titanium.

1.6 Titanium dioxide nanotubes

1.6.1 Applications and properties of Titanium Dioxide Nanotubes

The first self-organized TNTs on titanium were reported when Zwilling et al. used hydrogen fluoride solution in an electrolyte in 1999 (Regonini, Bowen, Jaroenworaluck, & Stevens, 2013). Over time with experimentation with different electrolyte compositions and applied voltages, it was found that the geometry of TNTs could be controlled. Their structure consists of open tops and closed scalloped bottoms. These tubes have diameters on the order of nanometers and have lengths that can go up to the order of microns. TNTs allow for high electron mobility and they have a high specific surface area.

Titanium dioxide nanotubes (TNTs) have a myriad of applications. These cylindrical shaped structures can be used in gas sensors, photocatalysis, dye-sensitized solar cells, photochromic devices, and biomedical devices (Roy, Berger, & Schmuki, 2011) (Lei, Luo, Sun, Kuang, & Su, 2013).

A University of California, San Diego group (Bjursten et al., 2010), has established that TNTs on implants promote osseointegration. A group from the University of California, San Francisco (Popat, Leoni, Grimes, & Desai, 2007), demonstrated the ability of nanotube surfaces to promote osteoblast differentiation. In a study by (Song, Schmidt-Stein, Bauer, & Schmuki, 2009), TNTs were used for controlled drug release.

TNTs have a wide band gap that is useful for applications related to solar cells and photocatalytic reactions. The resulting electron pairs from the photocatalytic reactions can be used for applications ranging from splitting water into oxygen and hydrogen to remediation of hazardous wastewater.

A variety of methods can be used to make TNTs, which include sol-gel techniques, hydro/solvothermal methods with or without templates, and ALD into templates (Roy et al., 2011). However, in this study, specific attention will be given to TNTs produced through electrochemical anodization with an organic electrolyte.

1.6.2 Electrochemical Anodization

In electrochemical anodization, a constant voltage source is applied to the electrolyte solution that houses the anode (the titanium) and cathode. The organic electrolyte (specifically ethylene glycol) consists of a fluoride source and an oxygen source. The fluoride source is usually ammonium fluoride. The oxygen source is usually distilled water.

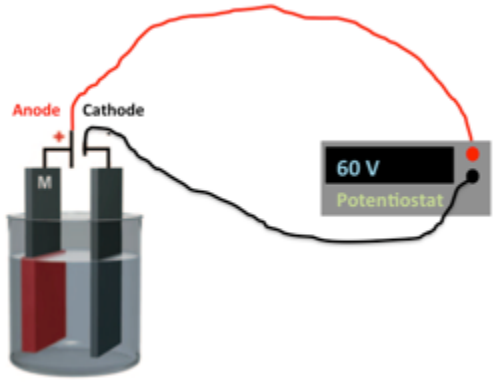

Figure 1.3 Metal (M) sample and the corresponding cathode in electrolyte solution and the anodization setup used in this study. The metal sample was titanium. The cathode used in this study was a copper rod. The voltage held by the potentiostat was 60 V (Roy et al., 2011).

At the anode, Ti^{4+} ions are released into the solution and oxidation occurs.

$$Ti \rightarrow Ti^{4+} + 4e^{-} \quad \text{.....Eqn. 1.3}$$

These ions combine with the OH^{-} and O^{2-} species from the DI water in the solution to form $Ti(OH)_4$ and TiO_2.

$$Ti^{4+} + 4OH^{-} \rightarrow Ti(OH)_4 \quad \text{.....Eqn.1.4}$$

$$Ti^{4+} + 2O^{2-} \rightarrow TiO_2 \quad \text{.....Eqn. 1.5}$$

Additional oxide forms when $Ti(OH)_4$ releases water in a condensation reaction.

$$Ti(OH)_4 \rightarrow TiO_2 + 2H_2O \quad \text{.....Eqn. 1.6}$$

At the cathode, hydrogen evolution occurs.

$$4H^+ + 4e^- \rightarrow 2H_2 \quad \text{.....Eqn. 1.7}$$

Thus the overall reaction for field-assisted oxidation is the following.

$$Ti + 2H_2O \rightarrow TiO_2 + 2H_2 \quad \text{.....Eqn. 1.8}$$

In the absence of fluoride ions, a compact oxide called the barrier layer forms (Roy et al., 2011). However, the pores that define the TNTs form due to field-assisted dissolution. In this process, the electric field weakens the bond between titanium and oxygen and the fluoride ions dissolve both the $Ti(OH)_4$ and TiO_2 and form soluble hexafluoride complexes, TiF_6^{2-}. TiF_6^2which is stable in solution.

$$TiO_2 + 6F^- + 4H^+ \rightarrow TiF_6^{2-} + H_2O \quad \text{.....Eqn. 1.9}$$

$$Ti(OH)_4 + 6F^- \rightarrow TiF_6^{2-} + 4OH^- \quad \text{.....Eqn. 1.10}$$

The fluoride ions also react with Ti^{4+} in solution.

$$Ti^{4+} + 6F^- \rightarrow TiF_6^{2-} \quad \text{.....Eqn. 1.11}$$

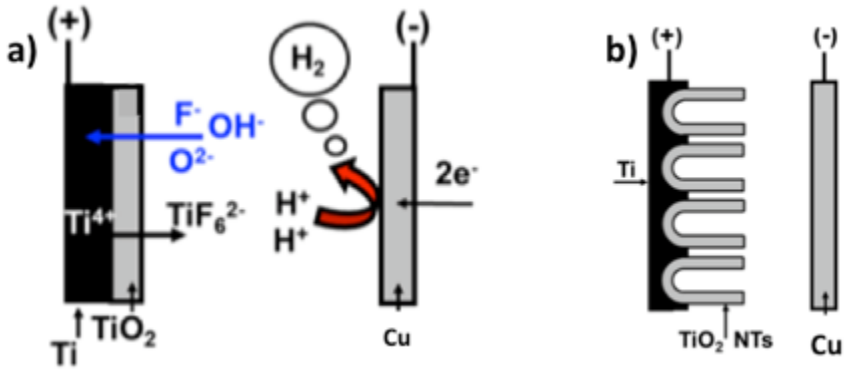

Figure 1.4 a) A schematic of the ions in the electrolyte solution; b) A depiction of the TNTs that form on the titanium sample during electrochemical anodization (Regonini et al., 2013).

The electric field is the strongest at the TNT base (Regonini et al., 2013). Due to this, the majority of TNT growth occurs at the pore base. As a result of the chemical reactions

described above, the resulting TNTs are made of two parts: a thin barrier inner layer at the metal/oxide interface, and a porous outer layer at the oxide/electrolyte interface.

1.6.3 Field-Assisted Flow Theory

There are theories on the mechanism by which titanium oxide transitions from a layer with shallow pits in the surface to fully formed cylindrical nanotubes. One such theory is called the field-assisted flow theory. This theory describes tubes growing due to the constant displacement of oxide from the barrier layer to the pore walls (Regonini et al., 2013). During the growth of the oxide layer, the oxide experiences stress due to electrostriction and volume expansion. Electrostriction is caused by displacement of ions in the oxide upon being exposed to an external electric field; positive ions are displaced in the direction of the field and negative ions are displaced in the opposite direction. The displacement accumulates throughout the bulk material and results in an overall strain and subsequent elongation.

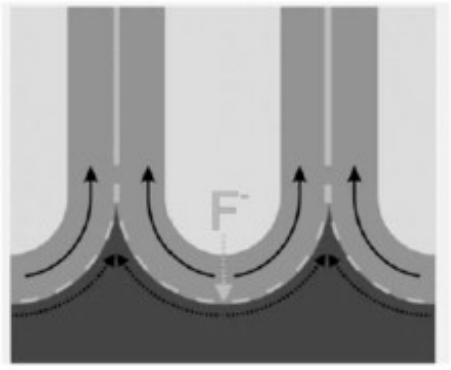

Figure 1.5 Titanium dioxide displacement from the barrier layer to the TNT pore walls (Roy et al., 2011).

1.6.4 Factors Affecting Titanium Dioxide Nanotube Growth and Geometry

Anodization voltage, time, and electrolyte composition allows for the customization of TNT pore diameter, wall thickness, and tube length.

Ion mobility in the electrolyte solution can be modeled using the Stokes-Einstein relation (Yin, Liu, & Shen, 2010),

$$D = \frac{k_B T}{6\pi\eta r} \quad \text{.....Eqn. 1.12}$$

This equation applies to the diffusion of spherical particles through a viscous liquid (low Reynolds number). In the equation, the D is the diffusion constant, k_B is Boltzmann's constant, T is absolute temperature, η is dynamic viscosity, and r is radius of the spherical particle. The addition of water decreases the viscosity of the solution and thus increases the diffusion of ions.

Increased temperature also results in increased diffusion of ions.

Using the electrolyte multiple times for anodization causes the $[TiF_6]^{2-}$ to build up in solution (Yoriya, Kittimeteeworakul, & Punprasert, 2012).

The increased mobility of ions and buildup of electrolyte conductivity causes increased chemical etching and oxide dissolution. This leads to larger pore diameters and smaller wall thicknesses of the nanotubes.

The applied potential used in anodization determines the electric field across the titanium oxide layer on titanium. This directs affects the migration of ions in solution. A higher applied potential causes higher ionic mobility and results in higher electrolyte conductivity. This leads to a larger pore size. There is a positive linear correlation between the applied potential and the internal and external diameters of titanium dioxide nanotubes (Roy et al., 2011).

1.7 Surface characterization techniques

1.7.1 Field Emission Scanning Electron Microscopy

Field emission electron microscopy (FESEM) is a powerful imaging tool in which electrons are used to probe objects on a very fine scale. Field emission refers to a cold source of electrons is being emitted from the surface of a conductor. This emission is caused by a strong electric field (Yao & Kimura, 2007). The field emission is combined with a scanning electron microscope. The electron beam produced by the field emission source is 1000 times smaller than that produced by a standard microscope, resulting in very high image quality (Yao & Kimura, 2007). Therefore, FESEM is a very useful technique for high-resolution surface imaging of TNTs.

1.7.2 Energy Dispersive X-ray Spectrometry

Energy dispersive X-ray spectrometry (EDS) is a chemical analytical technique. In this process, the sample to be analyzed is bombarded with a focused beam of electrons. The sample then emits an X-ray spectrum, which allows the analyst to do a localized chemical analysis. One can do a qualitative analysis by identifying the lines in the spectrum ("Introduction to Energy Dispersive X-ray Spectrometry (EDS)," 2014).

In EDS, the spatial resolution of the results depends on the penetration and spreading of the electron beam in the specimen. Ideally, the specimens should be well polished so that surface roughness doesn't affect the results. Therefore, this is not the best chemical analysis tool for TNTs, which have a rough surface. However, EDS is an efficient tool to analyze the chemical composition of TNT samples and it is often paired with FESEM systems.

1.7.3 White Light Interferometry

White light interferometry is a noncontact method of measuring surface roughness of samples. In this method, a white light passes through a filter and microscopic lens onto the sample to be analyzed. When the light reflects back from the surface of the sample, it recombines with the reference light beam. The recombined beams create bright and dark bands called fringes (Wyant, 2002). The fringes represent the object's topography. They are captured by a CCD camera and converted to digital data. The data is analyzed by the white light interferometry software to recreate the sample surface, complete with the height information. This height information yields the surface roughness information. The software uses the following formula to calculate the R_a, the arithmetic average of the absolute values of the roughness profile,

$$R_a = \left(\frac{1}{L}\right) \int_0^L |z(x)|\, dx \qquad \text{.....Eqn. 1.13}$$

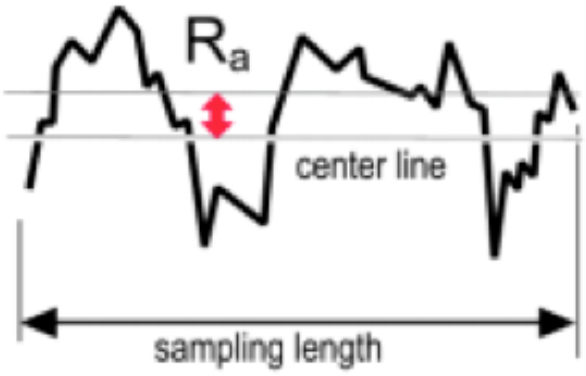

Figure 1.6 Visual depiction of the meaning behind R_a ("Surface Texture Parameters").

1.9 Summary & Objective

Much is known about PFMs and the materials that individually make up PFMs: titanium and porcelain. Titanium has superb mechanical properties, is biocompatible, and

is cost-effective. The low-fusing porcelain typically used with titanium has a CTE value very similar to that of titanium. When ceramic is deposited on titanium and fired in a dental furnace, it becomes highly reactive and a nonadherent oxide scale forms at the interface. Chemical coatings on titanium continue to be investigated as barriers to the titanium oxide formation during the firing process. However, current literature lacks the investigation of using TNTs as a an intermediate to produce mechanical interlocking between the titanium and dental porcelain. This study aims to evaluate if growing TNTs on titanium and subsequently adding dental porcelain leads to stronger bonding strengths.

Chapter 2

On the Bonding between TiO_2 Nanotubes and Dental Porcelain

Abstract:

The objective of this study is to strengthen the bonding between titanium and dental porcelain. The hypothesis is that titanium dioxide nanotubes (TNTs) grown on titanium will increase the mechanical interlocking between the dental porcelain and the underlying metal. TNTs of different lengths were formed on commercially pure (grade 2) titanium and Ti6Al4V (grade 5) samples via electrochemical anodization by varying the anodization time. Dental porcelain was added onto the titanium and the metal-ceramic samples were subsequently fired in a dental furnace. The bond strength of these samples was evaluated using the 3-point bending method and the results were analyzed using the student t-test. The results showed that the anodized samples did not have higher debonding strengths than the non-anodized controls. In fact, a few of the anodized metal-ceramic samples showed significantly lower debonding strength values compared to the controls. TNTs became deformed during the porcelain firing process due to the exposure to high temperatures in the dental furnace. These findings suggest that there is a need for a different strategy to successfully achieve stronger bonding between the titanium and dental porcelain.

2.1 Introduction

Historically, gold has been the preferred metal of choice for dental restorations. This is because of its excellent bond strength to dental porcelains (Lim, Kim, Lee, & Park, 2011). However, the price of gold has steadily increased to the point where cheaper materials are sought after for dental restorations. Base metals (NiCr, CoCr) have been evaluated as

replacements for gold (Yilmaz & Dinçer, 1999) (Akova, Ucar, Tukay, Balkaya, & Brantley, 2008) (de Melo, Travassos, & Neisser, 2005), but they have significant disadvantages when used in dental restorations; they have poor biocompatibility and low corrosion resistance, and they cause discoloration of porcelain (Yilmaz & Dinçer, 1999) (Powers, 2012).

Titanium and titanium alloys have many positive attributes, which make them attractive for use in dental restorations. They have excellent corrosion resistance (Lim et al., 2011) (Khung & Suansuwan, 2013), high strength (Lim et al., 2011) (Park et al., 2009), high microhardness (Lim et al., 2011) (Park et al., 2009), are biocompatible (Suansuwan & Swain, 2003) (Khung & Suansuwan, 2013), and are of low cost (Adachi, Mackert, Parry, & Fairhurst, 1990).

The nonadherent oxide layer that forms on titanium from the high heat exposure during the porcelain firing process is one of the factors for why titanium metal is not as stable in dental restorations as the nonreactive gold (S. Park et al., 2009). Various pure metals and ceramics have been used to coat titanium surfaces before the application of porcelain in order to prevent this excessive titanium oxidation. These coatings serve as barriers to oxygen diffusion into the titanium. Gold has been used to coat titanium through a sputtering technique (Park et al., 2009) (Khung & Suansuwan, 2013) (Lim et al., 2011). The gold-coated titanium has displayed higher bonding strength than uncoated titanium and even titanium coated with different materials. Zirconium silicon nitride (ZrSiN) coatings with different amounts of silicon have been tested on titanium (Zhang et al., 2014). The coating with the highest atomic percentage of silicon (18 at. %) has displayed the strongest bond with porcelain in this case. Titanium nitride (TiN) (Park et al., 2009), Calcium stabilized zirconia (ZrO_2-CaO) and nickel-aluminum-molybdenum + calcium

stabilized zirconia (Ni-Al-Mo+ ZrO_2-CaO) (Marcelli et al., 2014), and silicon nitride (Si_3N_4) (Wang, Welsch, & Monteiro, 1999) are among some other coatings that have successfully increased the bonding between titanium and porcelain. These are purely chemical means to increase the bonding between the metal and ceramic. Since porcelain is a molten glass during the firing procedure, it is chemically dissimilar to the underlying metal. As a result, no true adhesion can be obtained solely from chemical van der Waals forces. Mechanical retention through roughening the metal surface by abrasion or etching can be used to obtain interlocking between the metal and ceramic (Darvell, 2009).

A previous study has been done to evaluate the effects of a nanoporous film on the bonding strength between grade 2 titanium and porcelain (Guo et al., 2013). In this work, the nanoporous film was created by electrochemical anodization. The anodized samples had 200 nm diameter pores. Porcelain was applied on the anodized samples and the finished samples were subjected to a 3-point bending test. All conditions were set to ISO 9693 standards. The investigators concluded that the group of anodized samples showed a 7% improvement in bonding strength compared to the control group due to the mechanical interlocking effect. Since nanotubes have more surface area than nanopores, we hypothesize that the porcelain will have even more contact area with the nanotubes grown on titanium and increase its adhesion to the metal.

Titanium dioxide nanotubes (TNTs) have a myriad of applications ranging from the biomedical to the electronic. TNTs can be grown on titanium orthopedic implants to promote osseointegration (Dong Hwan Shin, 2011) (Hamlekhan et al., 2014) (Patel et al., 2014) (Bjursten et al., 2010) (Popat, Leoni, Grimes, & Desai, 2007). TNTs can also be used for controlled drug release applications (Shokuhfar, Sinha-Ray, Sukotjo, & Yarin, 2013)

(Song, Schmidt-Stein, Bauer, & Schmuki, 2009). They can be used in nanoscale electronic and optoelectronic devices as well as in solar cell applications because of their electron transport properties (Asthana et al., 2010).

TNTs grown on titanium are thought to increase the metal's adhesion to the porcelain on top. Before the porcelain is fired, the majority of dental porcelain particles are 10-20 μm (Rasmussen, Ngaji-Okumu, Boenke, & O'Brien, 1997). Since the nanotube diameters grown on titanium are only on the order of nanometers, it is unlikely that the room-temperature porcelain particles are able to go inside nanotubes. Although dental porcelains do not have a definite melting temperature, they undergo a gradual decrease in viscosity when heated (O'Brien, 1997). The greatest decrease in viscosity occurs around the glass-transition temperature (T_g). Above the T_g, the glass flows more readily and sintering takes place. During sintering, the porcelain particles consolidate and form a solid mass without melting to the point of liquefaction (Bergmann & Stumpf, 2013). The hypothesis for this study was that as the porcelain became less viscous, it would soften into the nanotubes of the samples thus creating a mechanical interlocking effect, which would increase the porcelain's adhesion to the titanium.

The objective of this study is to strengthen the bonding between titanium and dental porcelain. The ultimate aim of this work could be to reduce the price of the metal used in dental restorations while preserving their longevity.

2.2 Materials and Methods

2.2.1 Experimental Design

The groups were organized as shown in table 2.1. They differed in the grade of titanium and the duration of anodization. There were 10 samples in each group.

Table 2.1 Organization of grade 2 and 5 titanium groups with respect to the amount of time they were anodized in an electrolyte solution composed of ethylene glycol, 0.2 wt. % NH_4F, and 4 wt. % DI water at 60V. The load at which the samples debonded from the porcelain (F_{fail}) and the corresponding calculated debonding strengths (τ_b) are listed for each group.

Group no.	Grade of titanium	Anodization duration (min)	F_{fail} (N)	τ_b (MPa)
1	2	0	4.7±0.66	16±2.4
2	2	1	3.7±0.54	12±1.2
3	2	3	*	*
4	2	5	4.8±0.80	16±2.5
5	2	15	4.1±0.93	13±2.6
6	2	30	3.9±0.89	14±2.7
7	5	0	5.1±0.60	17±3.0
8	5	1	2.8±0.76	11±3.0
9	5	3	*	*
10	5	5	5.4±0.58	19±3.0
11	5	15	4.7±0.49	15±1.6
12	5	30	4.2±0.44	15±2.4

* Did not test this sample

2.2.2 Sample Preparation

The titanium samples were cut into rectangular shapes from grade 2 and grade 5 titanium sheets. Their dimensions matched the ISO standard specifications: 25±1 mm × 3±0.1 mm × 0.5±0.05 mm.

To follow current dental practices and create micro-scale surface roughness, the samples were sandblasted with 50 μm alumina particles at a 90° angle from a distance of 30 mm from the sample, for 10 seconds, at an air pressure of 200 kPa. To create nano-scale surface roughness, the samples were acid-etched in sulfuric acid and 30% hydrogen peroxide (solution mixture, volume ratio 1:1) for two hours.

The samples were cleaned by sonication in 200 proof (100%) ethanol (Decon Labs, Inc., King of Prussia, PA, USA) and DI water separately for 15 min in each solution.

2.2.3 Electrochemical Anodization

The samples were anodized in order to obtain nanotubes on their surfaces. The titanium samples served as the working electrodes and a copper rod was used as the counter electrode in the anodization process. Both electrodes were connected to a voltage source (Keithley 2400 SourceMeter, Cleveland, OH, USA) and immersed in an electrolyte solution composed of ethylene glycol (Fisher Scientific, Pittsburgh, PA, USA), 0.2 wt. % NH_4F (Sigma-Aldrich, St. Louis, MO, USA), and 4 wt. % DI water. 60 V was maintained for the anodization time the samples were subjected to as is listed in table 2.1. The current with respect to time was recorded. In all of the anodization experiments, the average distance between the counter electrode and the titanium samples was 3 cm. The electrolyte solution was continuously stirred to maintain a homogeneous environment. After the samples were anodized, they were cleaned by sonication in ethanol and DI water separately for 15 min in each solution.

2.2.4 Surface Characterization

Field emission scanning electron spectroscopy (FESEM; JSM-6320F, JEOL, Musashino 3-chome Akishima Tokyo, Japan) was used to image the top of the samples. FESEM images were taken of the samples to view their surface morphology and measure nanotube dimensions. To measure the top view of nanotubes on the anodized samples, the samples were placed on double-sided conductive carbon tape and attached to aluminum stubs for imaging in FESEM. In order to measure the lengths of the nanotubes on the anodized samples, detached bundles of nanotubes were placed on double-sided conductive carbon tape in a similar fashion as described above. ImageJ software was used to measure the inner diameter and lengths of the nanotubes.

Energy-dispersive X-ray spectroscopy (EDS) analysis was done on the anodized grade 2 and grade 5 samples to analyze the chemical composition of the TNTs. EDS was done using the FESEM device equipped with the EDS detector (JEOL JSM-6320F detector).

In order to quantify the surface roughness of the samples, the average of the absolute value of sample roughness profiles was measured (R_a). A white light interferometer (NewView 3600, Zygo Corporation, Middlefield, Connecticut, USA) with 20X Mirau magnification was used to measure these values. The software used to access the roughness data was MetroPro Version 8.1.5 Copyright © 2005 (Zygo Corporation, Middlefield, Connecticut, USA).

2.2.5 Porcelain Stacking and Firing

The porcelain used in this study is VITA Titanium Porcelain (VITA Zahnfabrik H. Rauter GmbH & Co. KG, Bad Säckingen, Germany) and it has a coefficient of thermal expansion of 9.6×10^{-6}/°C.

Vita Titankeramik low fusing porcelain was stacked onto the titanium samples following the manufacturer's recommended firing schedule as shown in table 2.2. A paste bonding layer was added and then fired without vacuum (Jalenko Commodore II dental furnace). The opaque layer and dentin layers were fired under vacuum (72 cm Hg) to 790°C and 770°C, respectively.

The porcelain was added thicker than necessary and then polished to 1.1 mm thick using 400 grit silicon carbide sanding papers with water as the lubricant. The ends were squared up if necessary using a high speed handpiece with ultrafine carbide burs.

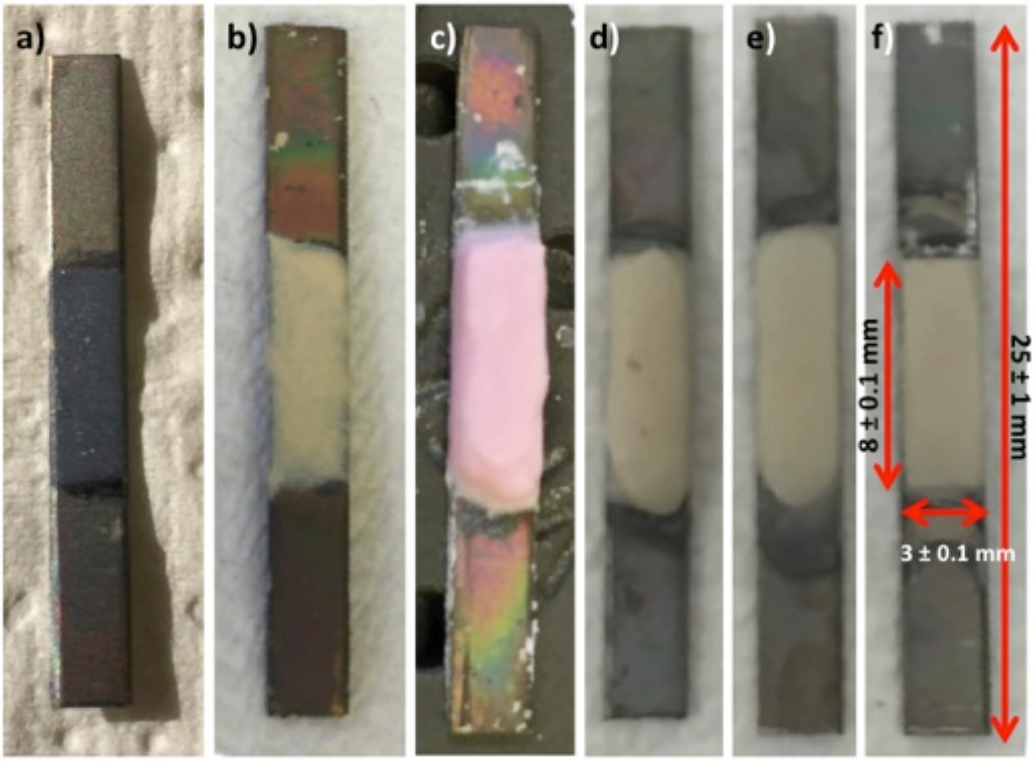

Figure 2.1 Titanium samples with a) bond layer applied; b) opaque layer applied; c) dentin layer. d) Metal-ceramic samples after firing in porcelain furnace, before shaping, e) after shaping, and f) after squaring off the ends with the high-speed handpiece. The titanium samples were 25 ± 1 mm long, 3 ± 0.1 mm wide and 0.5 ± 0.05 mm thick. The porcelain stacked on top of the titanium had dimensions of 8 ± 0.1 mm, 3 ± 0.1 mm, and 1.1 ± 0.1 mm.

Table 2.2 Firing schedules of VITA Titankeramik low fusing porcelain.

Layer	Paste Bonder	Opaque	Dentin
Low Temp (°C)	400	400	400
Preheat Time (min)	6	2	6
Heat Rate (°C/min)	67	98	53
Vacuum Level (cm Hg)	N/A	72	72
High Temp (°C)	800	790	770
Holding Time (min)	1	1	2*
Cooling Time (min)	2	5	8

*Extended holding time and cooling times as per manufacturer's suggestions due to combined bulk of samples.

2.2.6 Mechanical Testing

The bonding strength of the titanium-porcelain samples was measured using the 3-point bending test. The test was done using a universal testing machine (EZ graph, Shimadzu, Kyoto, Japan). All the samples subjected to the 3-point bending test rested on a jig with a support span of 20 mm, with the porcelain side facing opposite to the load being

applied. The support of the jig and bending piston had radii of 1.0 mm. The force was applied at a constant rate of 1.5±0.5 mm/min and was recorded until failure (F_{fail}) at which point the ceramic debonded from the titanium at one end of the ceramic layer. The software used to record all values was TestWorks®4 (MTS Systems Corporation, Eden Prairie, Minnesota, USA).

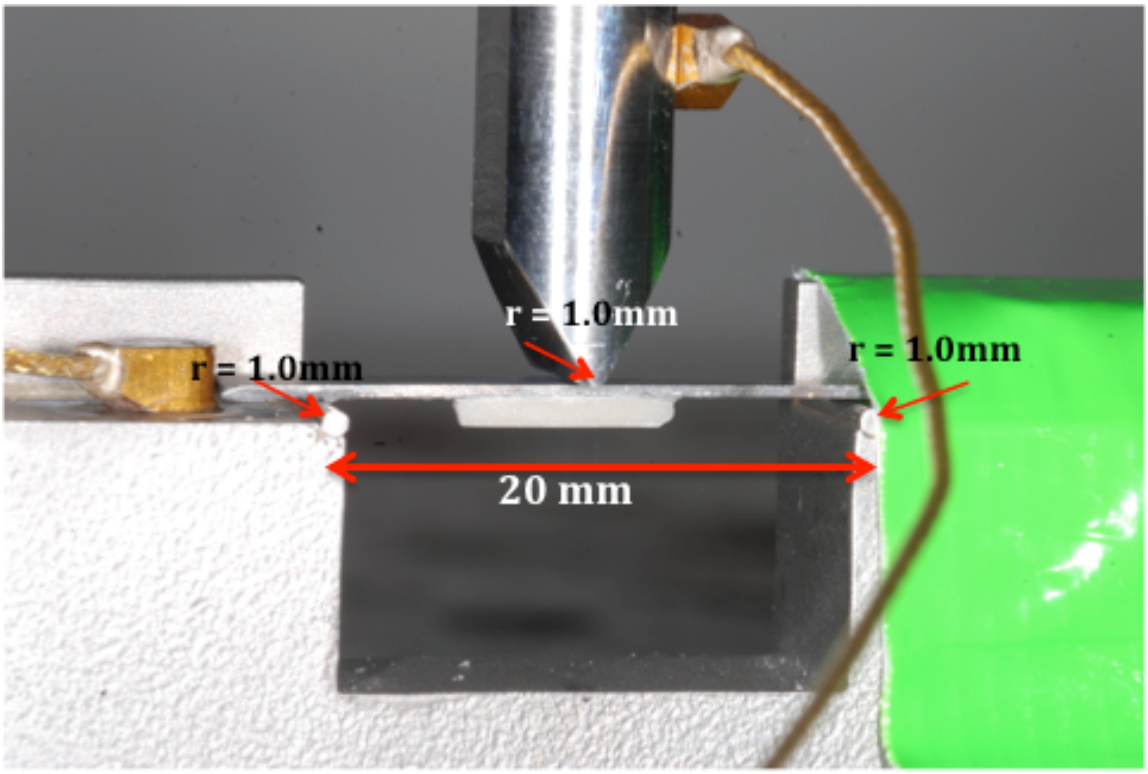

Figure 2.2 Jig used for 3-point bending test; it has a span of 20 mm between supports. It is capable of attaining a cross-head speed of 1.5 ± 0.5 mm. The supports and bending piston are rounded to have radii of 1.0 mm.

Evaluating debonding between titanium and ceramic

FESEM images were taken of the debonded titanium surfaces in order to evaluate the state of the TNTs after the 3-point bending tests. Titanium samples were placed on the double-sided conductive carbon tape and attached to aluminum stubs for imaging in FESEM. The titanium side that was attached to the porcelain was left facing up.

2.2.7 Statistical Analysis

The difference in the debonding strengths of grade 2 and grade 5 titanium samples was investigated statistically with 1-way ANOVA (α=0.05). In addition, the debonding strengths of the control grade 2 and grade 5 titanium samples were compared with that of their anodized counterparts using the student t-test.

2.3 Results & Discussion:

2.3.1 Surface Morphology of Samples

Atomic percentage composition TNTs grown on grade 2 titanium and grade 5 titanium as determined by EDS analysis are shown in Table 2.3. The compositions of the TNTs grown on different grades of titanium are similar with the exception of the aluminum present in grade 5 titanium. In accordance to previous studies, the main contaminants of the anodic nanotubes are fluoride and carbon (Regonini et al., 2013).

Table 2.3: Atomic % determined by FESEM-EDS analysis of TNTs grown on grade 2 and grade 5 titanium in electrolyte of ethylene glycol, 0.2 wt. % NH_4F, and 4 wt. % DI water at 60V.

Atomic % of Nanotubes on Grade 2 Titanium		Atomic % of Nanotubes on Grade 5 Titanium	
Titanium	67	Titanium	44
Oxygen	16.4	Oxygen	44
Fluorine	13.3	Fluorine	5.5
Carbon	3.1	Carbon	3.4
		Aluminum	3.0

FESEM images of the top views and lengths of the TNTs grown on grade 2 and grade 5 titanium are displayed in figs. 2.3 and 2.4. They show that the TNTs of various lengths and inner diameters were formed successfully during electrochemical anodization. Some of the nanotubes in the length images were broken by the scratching technique used while imaging them. The broken parts show the hollow interior structure of the TNTs (Zhao,

Wang, Chen, & Li, 2005). The length and inner diameter values of these TNTs are shown in figs. 2.5 and 2.6. Further discussion of the trends in these figures is below.

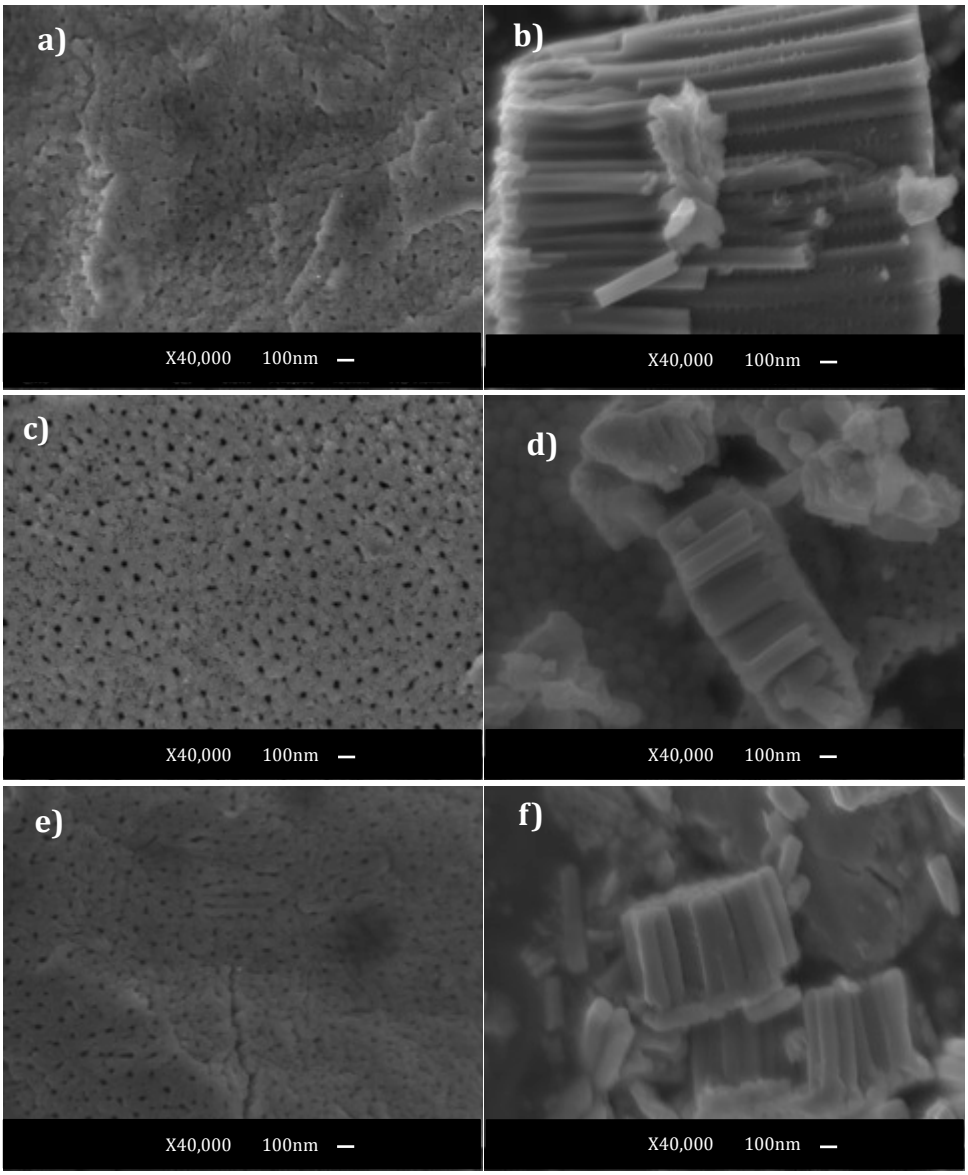

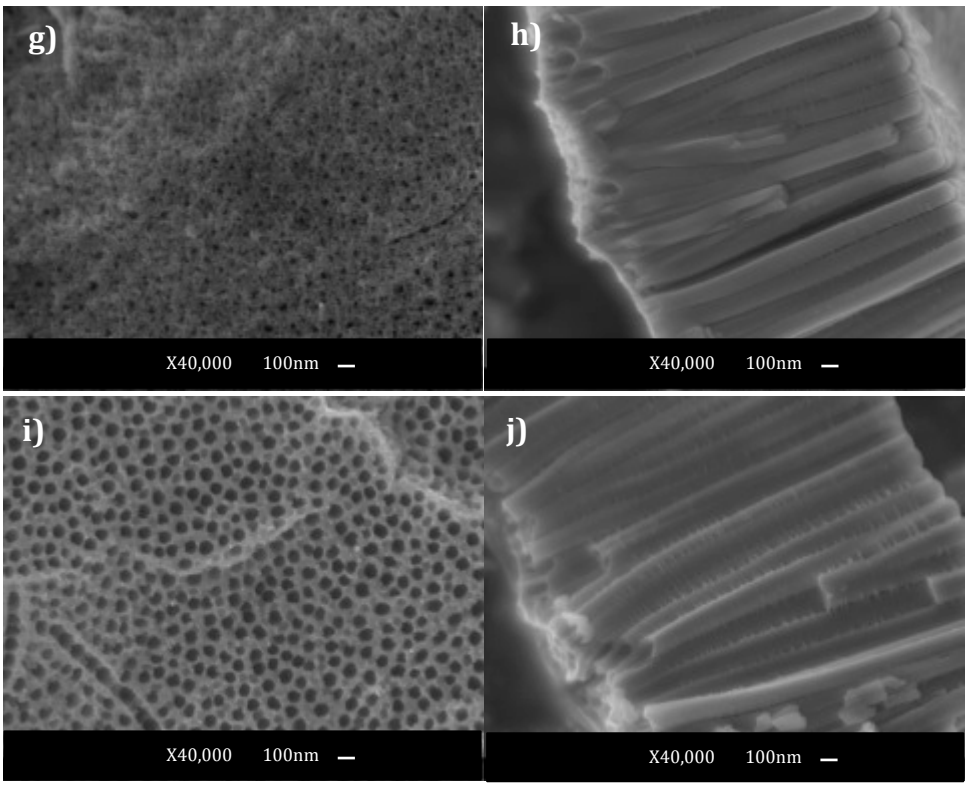

Figure 2.3 40X FESEM images of the top view and length of TNTs grown on grade 2 titanium; a) and b) 1 min anodization time; c) and d) 3 min anodization time; e) and f) 5 min anodization time; g) and h) 15 min anodization time; i) and j) 30 min anodization time. All samples were anodized in electrolyte of ethylene glycol, 0.2 wt. % NH_4F, and 4 wt. % DI water at 60V.

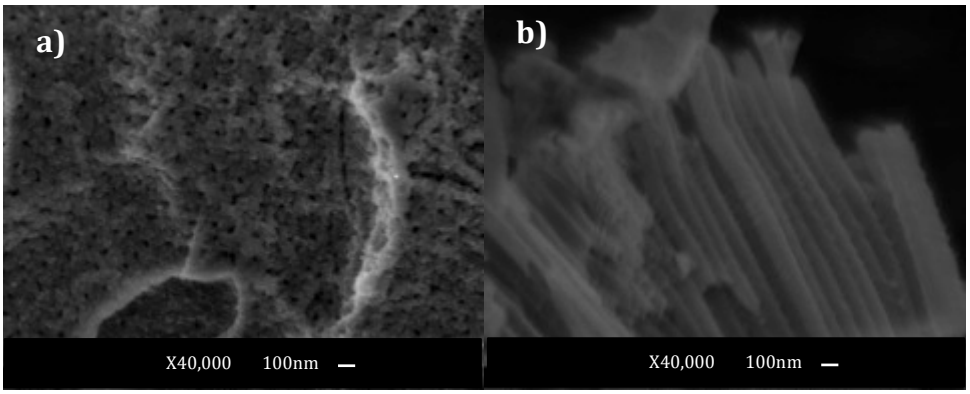

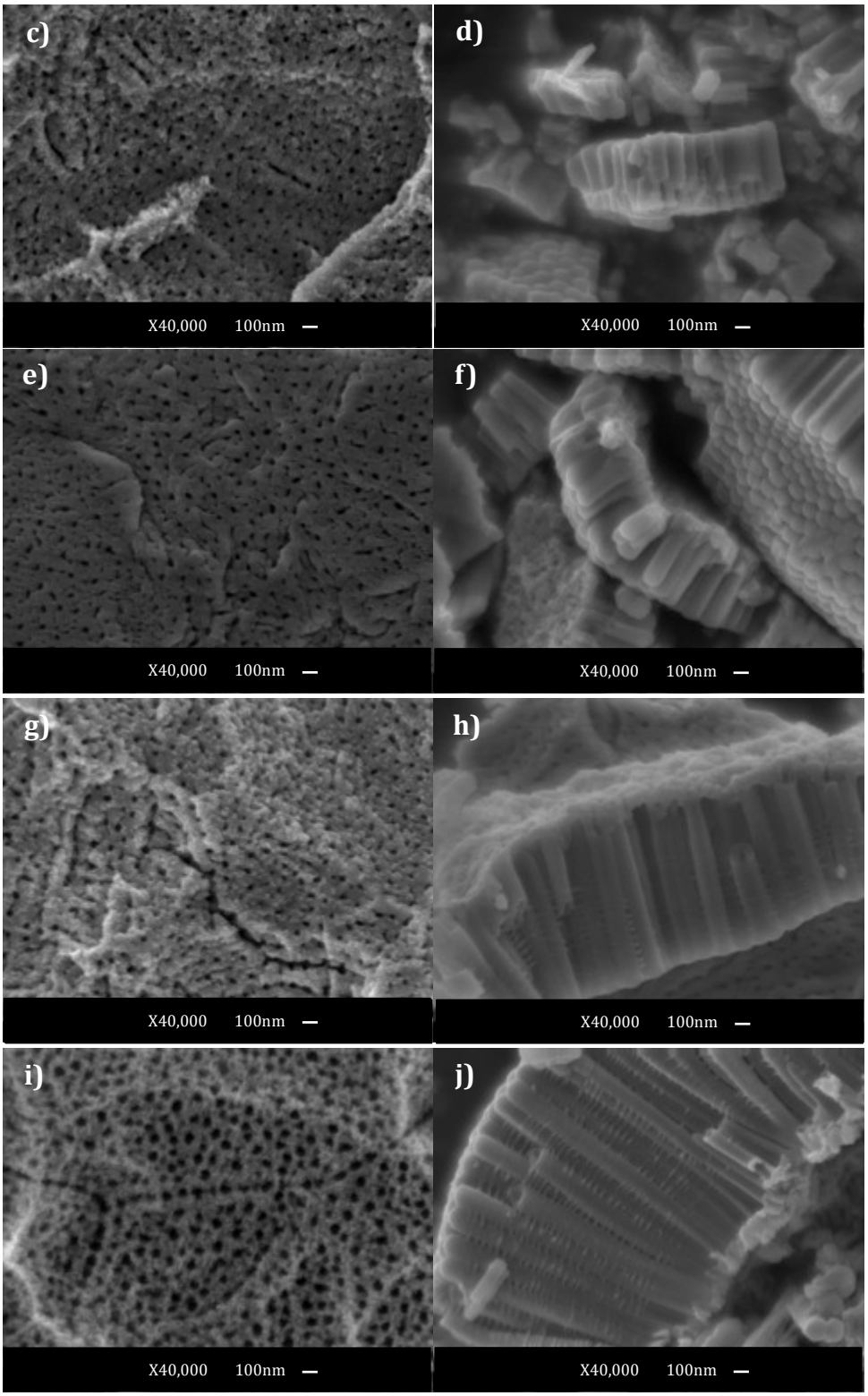

Figure 2.4 40X FESEM images of the top view and length of TNTs grown on grade 5 titanium; a) and b) 1 min anodization time; c) and d) 3 min anodization time; e) and f) 5 min anodization time; g) and h) 15 min anodization time; i) and j) 30 min anodization time. All samples were anodized in electrolyte of ethylene glycol, 0.2 wt. % NH_4F, and 4 wt. % DI water at 60V.

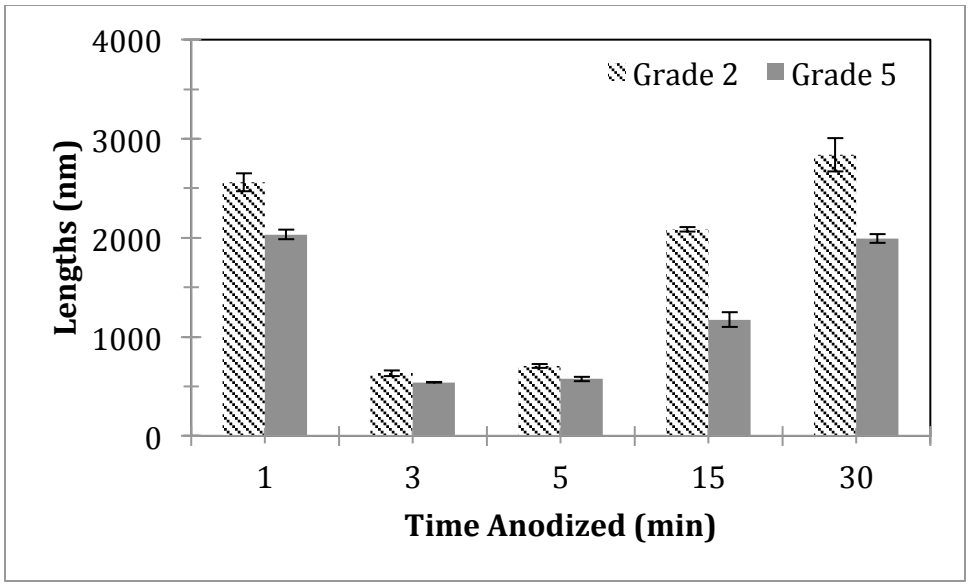

Figure 2.5 Length (nm) values measured from FESEM images of the grade 2 and grade 5 titanium samples anodized for 0, 1, 3, 5, 15, and 30 min in electrolyte of ethylene glycol, 0.2 wt. % NH_4F, and 4 wt. % DI water at 60V.

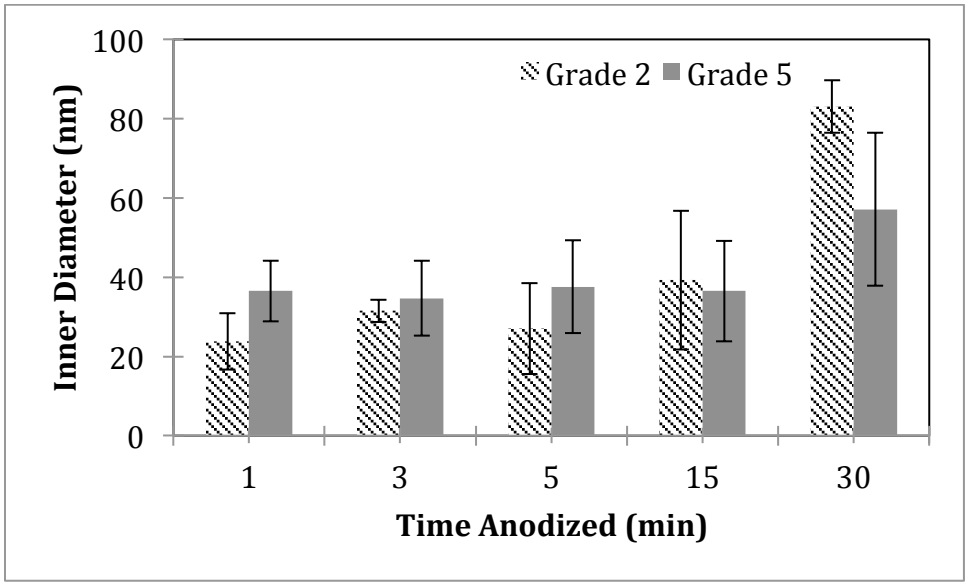

Figure 2.6 Inner diameter (nm) values measured from FESEM images of the grade 2 and grade 5 titanium samples anodized for 0, 1, 3, 5, 15, and 30 min in electrolyte of ethylene glycol, 0.2 wt. % NH_4F, and 4 wt. % DI water at 60V.

For both grade 2 and grade 5 samples, the lengths of the nanotubes that were anodized for 1 min were higher than the lengths of the nanotubes that were anodized for 3 min (fig. 2.5). The lengths of the nanotubes that were anodized for 3 min and 5 min were similar. The lengths of the nanotubes increased with anodization time for the 15 min and 30 min anodization times.

Typical growth of nanotubes has been reported as following three major stages, as detailed in fig. 2.7. The different stages correspond to the behavior of current density versus time during the electrochemical anodization process. In the first stage, the current density drops from its highest value to a minimum. According to previous studies (Regonini, Bowen, Jaroenworaluck, & Stevens, 2013) (Roy, Berger, & Schmuki, 2011), the current density decrease is a result of the rapid growth of an oxide layer on the titanium, which increases the resistance. The titanium ions go through oxidation reactions; they combine with OH^- and O^{2-} ions from the DI water in the solution to form TiO_2 and $Ti(OH)_4$ (Regonini et al., 2013) (Roy et al., 2011). This oxide layer is depicted in fig. 2.7. In the second stage, the current density begins to rise and reaches a local maximum point. This behavior is brought on by pores starting to form in the oxide layer. The pore nucleation, also shown in fig. 2.7, coincides with a decrease in the resistance of the oxide layer. The oxide dissolution is caused by the fluoride ions in solution dissolving TiO_2 and $Ti(OH)_4$ to create $[TiF_6]^{2-}$ ions (Regonini et al., 2013) (Roy et al., 2011). The current density then decreases and plateaus to a constant value in the third stage of the characteristic transient current behavior of titanium electrochemical anodization. This is indicative of the oxidation and dissolution forces reaching a steady state (Regonini et al., 2013) (Roy et al., 2011), with a net growth of TNT length (shown in fig. 2.7). During electrochemical anodization, the majority of TNT growth occurs at the TNT pore base where the electric field is strongest (Regonini et al., 2013). Titanium dioxide is consumed at a higher rate near the bottom of the pore, which results in TNT growth towards the titanium substrate (Zhao et al., 2005).

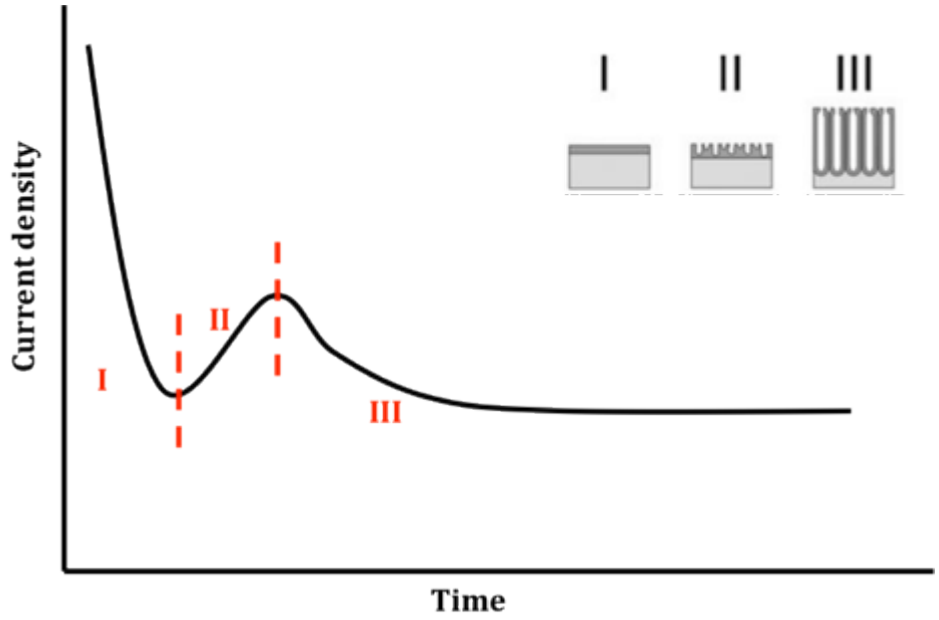

Figure 2.7 Typical current density-time characteristics of electrochemical anodization process with fluoride ions in the electrolyte. Figure modified from (Roy et al., 2011).

The current density was monitored with respect to time for both types of titanium in order to lend more insight into the length measurements. The formation of TNTs is due to the competition between electrochemical oxidation and chemical and field-assisted dissolution (Yang & Pan, 2010) (Regonini et al., 2013). Figs. 2.8 and 2.9 show the current density with time for anodizing grade 2 and 5 titanium at a constant voltage of 60 V in ethylene glycol electrolyte at 0.2 wt. % NH_4F and 4 wt. % DI H_2O. Both Figs. 2.8 and 2.9 show the same current density trend with respect to time as fig. 2.7 does. The length of the TNTs on both grade 2 and grade 5 titanium samples was long (fig. 2.5) at 1 min of anodization time when the current density was at a minimum. At this time, since the current density was at a minimum, it is clear that a large amount of oxide was present on the titanium.

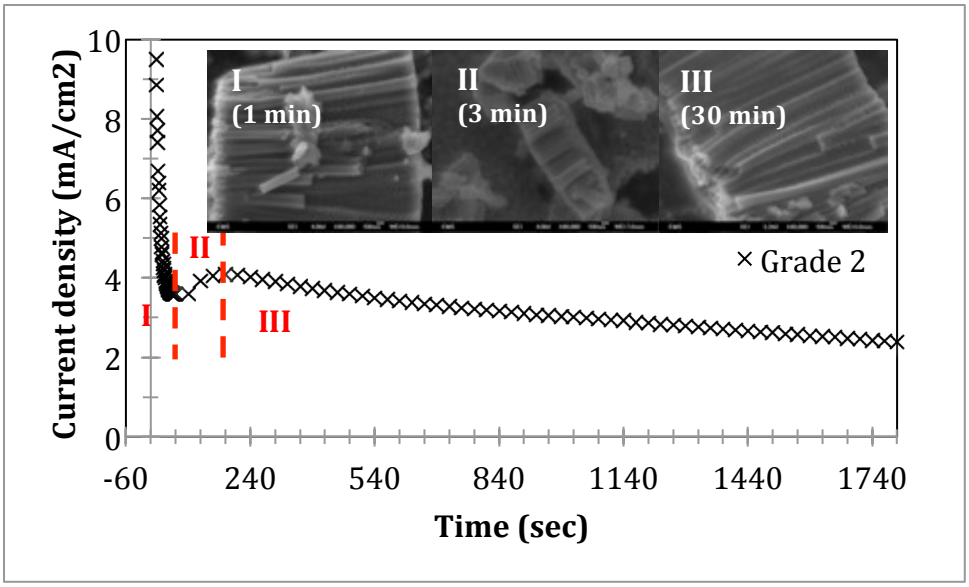

Figure 2.8 Current-time plot of electrochemical anodization process of grade 2 titanium sample in electrolyte of ethylene glycol, 0.2 wt. % NH_4F, and 4 wt. % DI water at 60V.

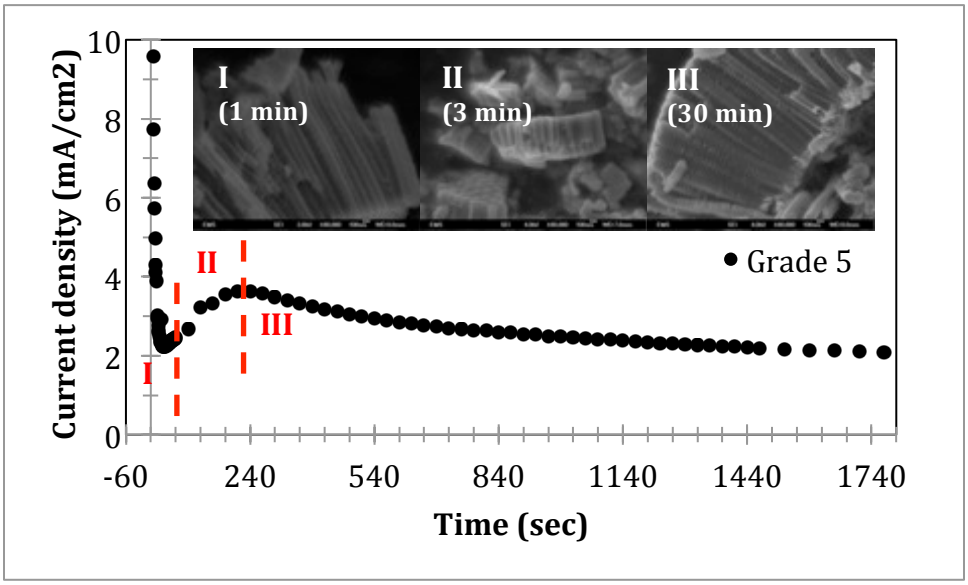

Figure 2.9 Current-time plot of electrochemical anodization process of grade 5 titanium sample in electrolyte of ethylene glycol, 0.2 wt. % NH_4F, and 4 wt. % DI water at 60V.

Previous studies that have monitored current density with respect to time have used either a sweeping voltage to build up to the final voltage, or a constant voltage. In both cases, the resulting voltage was relatively low: ~20-40 V (Berger et al., 2009) (Gong et al., 2001) (Zhao et al., 2005) (Mor, Varghese, Paulose, Mukherjee, & Grimes, 2003). In this study, the titanium samples were subjected to a constant voltage of 60 V from the start.

Since the electric field is proportional to the voltage (Regonini et al., 2013), the relatively high 60 V causes a strong electric field across the samples. The electric field is known to weaken the bond between titanium and oxygen in the oxide layer in a process called field-assisted dissolution, thus adding to the already existing process of the chemical dissolution of TiO_2 and $Ti(OH)_4$ by F^-(Regonini et al., 2013) (Yang & Pan, 2010). The applied electric field also drives Ti^{4+} ions from the titanium substrates towards the electrolyte and F^- ions towards the titanium-(Regonini et al., 2013) (Roy et al., 2011). Thus, F^- ions dissolve $Ti(OH)_4$ and TiO_2 and react with Ti^{4+} ions to form TiF_6^{2-}. F^- ions migrate twice as fast as O^{2-} ions through the oxide layer (Roy et al., 2011). Therefore, the action of F^- ions to burrowing through the oxide leads to the formation of nanotubes on the titanium samples even after only 1 min of anodization time.

The short length of the TNTs on both grade 2 and grade 5 titanium samples at 3 and 5 min of anodization match up with the local current density maximum. The rise in current density signals that the dissolution rate was higher than the oxidation rate. Therefore, the chemical etching of the TNT walls could have likely led to their shorter length.

The length of the TNTs increased again at 15 and 30 min of anodization time. This overlaps with the current density steadily decreasing and reaching a plateau. The dissolution rate and oxidation rates were reaching equilibrium at these times, with a net growth of TNT length.

The inner diameters of the tops of nanotubes (fig. 2.6) on the grade 2 and grade 5 anodized samples remained constant until 15 min of anodization time, at which point the average inner diameter of the nanotubes grew larger. Early on in anodization, chemical dissolution was not able to remove the top of the TNTs due to the low fluoride

concentration (~0.12 M) (Yang & Pan, 2010). According to (Yang & Pan, 2010), a fluoride concentration less than 2 M will hinder chemical dissolution from removing the top of TNTs at short anodization times. This resulted in the inner diameter of the tops of nanotubes (fig. 2.6) on the grade 2 and 5 anodized samples remaining constant until 15 min of anodization time. Both oxidation and chemical dissolution were active at the bottom of pores during the anodization process and formed tubes (Yang & Pan, 2010) (Regonini et al., 2013) as is apparent from the length images in figs. 2.3(b, d, f, h, and j) and 2.4(b, d, f, h, and j). With time, further chemical dissolution removed the top of the oxide of growing TNTs to result in open tube tops (Yang & Pan, 2010) as can be seen in figs 2.3i and 2.4i. White light interferometry was used to measure the roughness values of the samples. In white light interferometry, light is divided into two paths. One path shines on the substrate of interest and the other shines on a reference surface (Patel et al., 2014) (Wyant, 2002). When the light reflects back from the sample, it recombines with the reference light beam (Patel et al., 2014) (Wyant, 2002). The resulting information from the interference of the two light paths yields information about the object's topography (Patel et al., 2014) (Wyant, 2002). Despite the variance in lengths and inner diameters, the roughness values for all the samples ranged between 1 and 2 μm, as are shown in fig. 2.10. The roughness (R_a) of the control titanium samples that did not have any nanotubes on them was not significantly different than the R_a of the samples with nanotubes. This could be due to the fact that all the samples were sandblasted with 50 μm alumina particles. The macro-level roughness created by the alumina particles could have prevented the nano-level roughness created by the growth of TNTs, which had the lengths up to only ~2 micron (fig. 2.5), from showing up in the roughness measurements. A more detailed view of the surfaces of the

grade 2 and grade 5 titanium samples is showed in figs. 2.11 and 2.12. Figs. 2.11a and 2.12a, images of the control samples, are both less densely populated with the marks signifying the rough topography of the samples compared to figs. 2.11b and 2.12b, images of the samples that were anodized for 1 min. This increase in topography density could be caused by the formation of TNTs on the samples. Figs. 2.11(b, c, and d) and 2.12(b, c, and d), images of the samples anodized for 1, 3, and 5, are less densely populated with the marks compared to figs. 2.11(e and f) and 2.12(e and f), images of the samples anodized for 15 and 30 minutes. This increase in density could be caused by the open tube tops, shown in figs. 2.3(g and i) and 2.4(g and i), of the TNTs at 15 and 30 min of anodization compared to the more closed up tube tops, shown in figs. 2.3(a, c, and e) and 2.4(a, c, and e) of the TNTs at 1, 3, and 5 min of anodization. The not so open tube tops of the TNTs resulting from 1, 3, and 5 min of anodization could have blocked the opening of the TNTs and restricted the light from the white light interferometer from going inside the TNTs (Patel et al., 2014). This could have caused the lower density of topographical features in figs. 2.11(b, c, and d) and 2.12(b, c, and d). The open TNTs at anodization times of 15 and 30 min allowed the light from the white light interferometer to go inside the TNTs and led to the increase in density of topographical features in figs. 2.11(e and f) and 2.12(e and f).

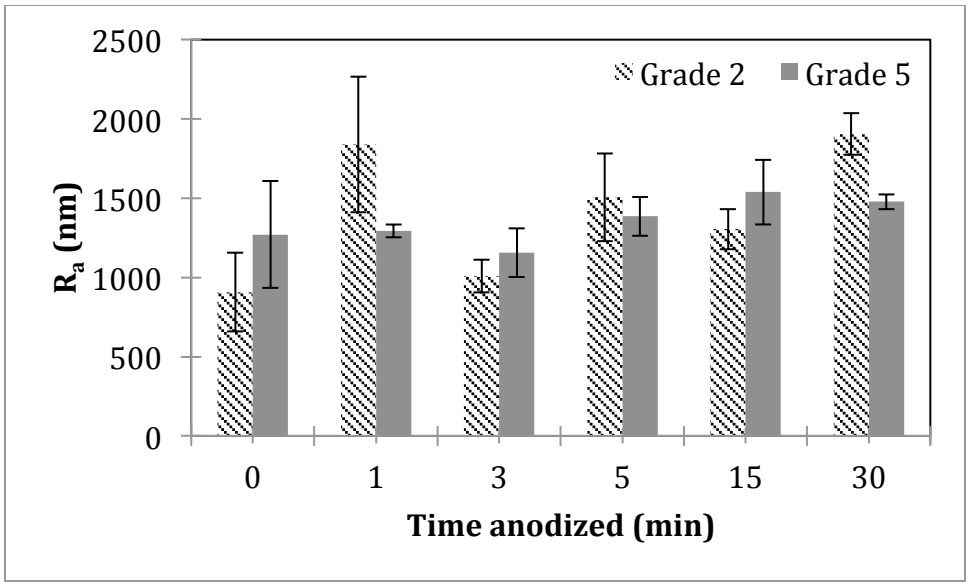

Figure 2.10 Average roughness, R_a, (nm), determined by white light interferometry of the grade 2 and grade 5 titanium samples anodized for 0, 1, 3, 5, 15, and 30 min (n=3) in electrolyte of ethylene glycol, 0.2 wt. % NH_4F, and 4 wt. % DI water at 60V.

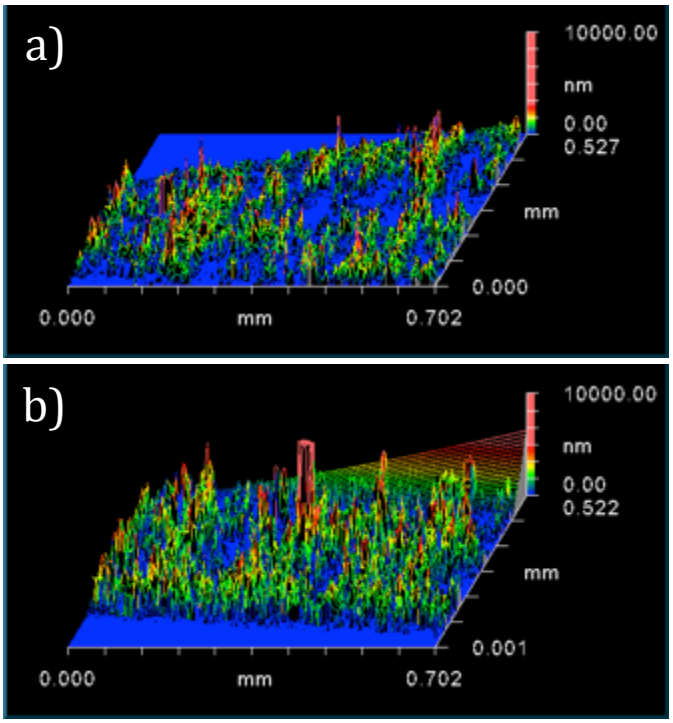

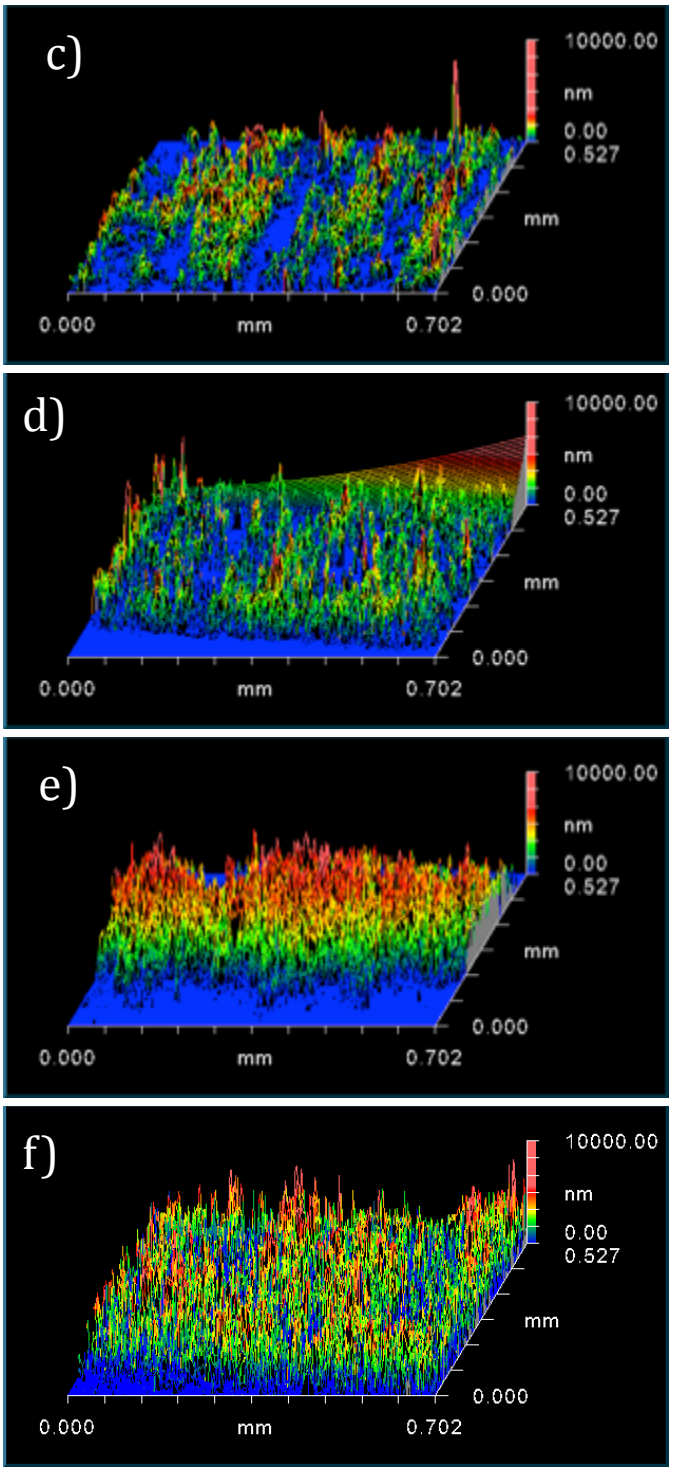

Figure 2.11 3-D Oblique Plots generated by MetroPro software from white light interferometry measurements. These plots represent the topography of the grade 2 titanium samples anodized for a) 0, b) 1, c) 3, d) 5, e) 15, and f) 30 min in electrolyte of ethylene glycol, 0.2 wt. % NH_4F, and 4 wt. % DI water at 60V.

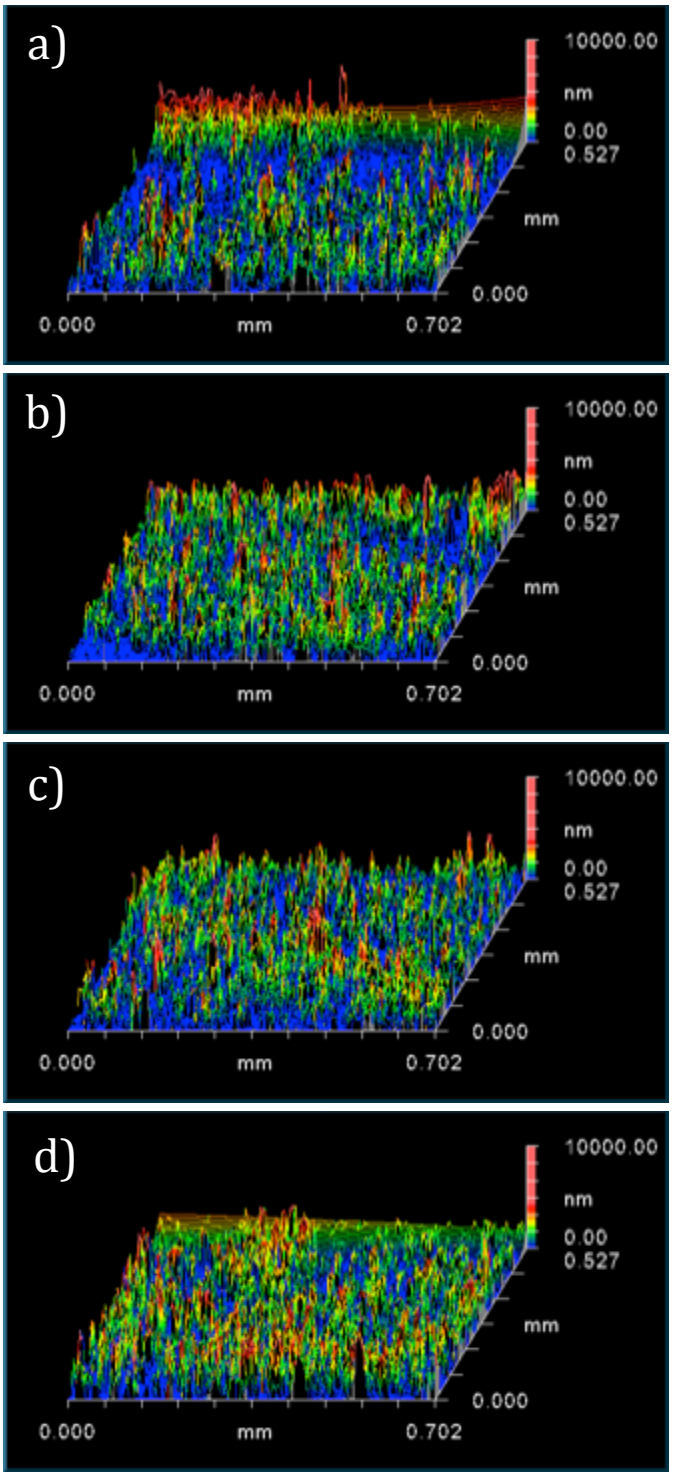
a)
10000.00
nm
0.00
0.527
mm
0.000
0.000
mm
0.702
b)
10000.00
nm
0.00
0.527
mm
0.000
0.000
mm
0.702
c)
10000.00
nm
0.00
0.527
mm
0.000
0.000
mm
0.702
d)
10000.00
nm
0.00
0.527
mm
0.000
0.000
mm
0.702

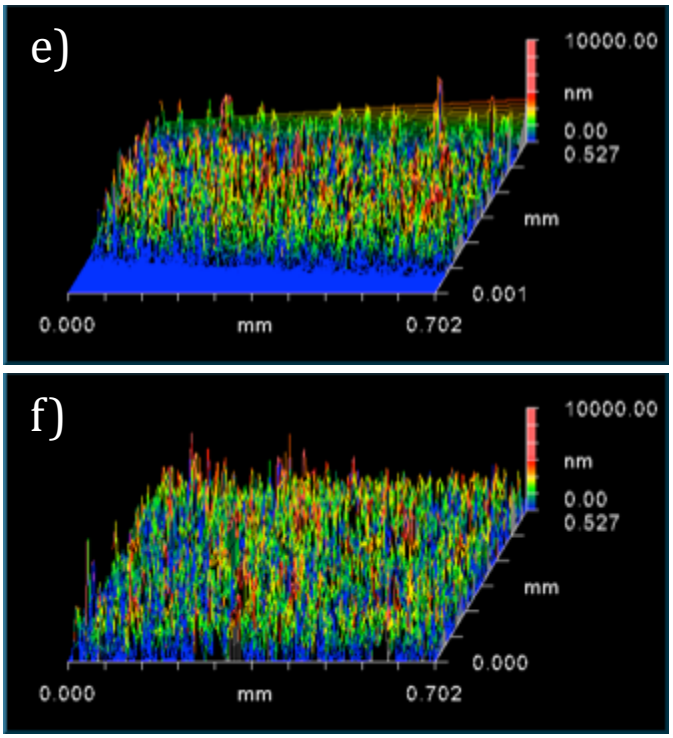

Figure 2.12 3-D Oblique Plots generated by MetroPro software from white light interferometry measurements. These plots represent the topography of the grade 5 titanium samples anodized for a) 0, b) 1, c) 3, d) 5, e) 15, and f) 30 min in electrolyte of ethylene glycol, 0.2 wt. % NH_4F, and 4 wt. % DI water at 60V.

2.3.2 Mechanical testing

From the data accumulated during the 3-point bending tests, the strength of the nanotube-dental porcelain bond was quantified using τ_b [MPa], which is shown in fig. 2.13 and table 2.1.

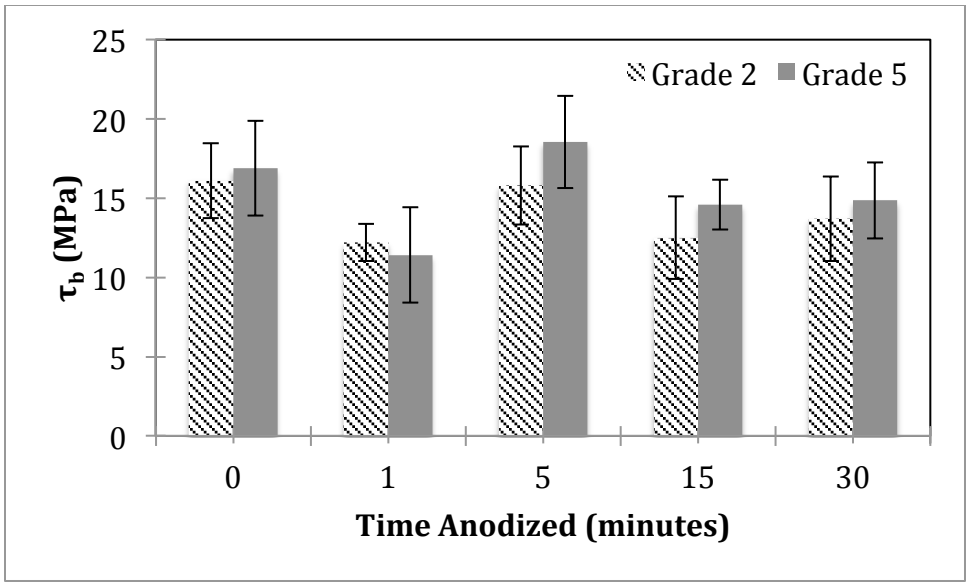

Figure 2.13 Calculated values of debonding strength, τ_b, (MPa) of the of the grade 2 and grade 5 titanium samples anodized for 0, 1, 3, 5, 15, and 30 min (n=10) in electrolyte of ethylene glycol, 0.2 wt. % NH_4F, and 4 wt. % DI water at 60V.

τ_b is the debonding/crack-initiation strength, and is calculated using the following equation:

$$\tau_b = k \times F_{fail} \quad \text{.....Eqn. 2.1}$$

F_{fail} [N] is the load at which the samples debonded and these values are shown in fig. 2.14 and in table 2.1.

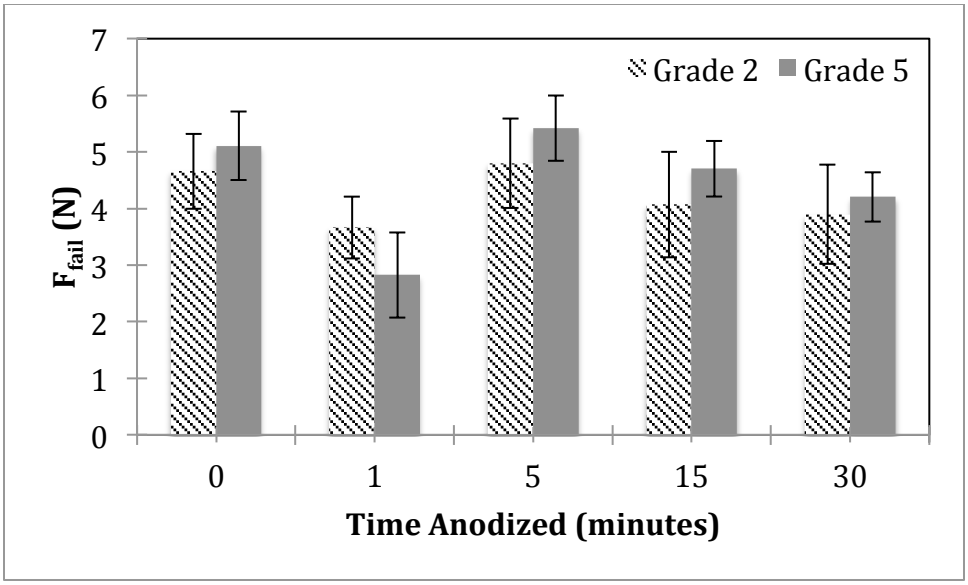

Figure 2.14 Load at which the metal-ceramic samples failed, F_{fail}, (N) when subjected to the 3-point bending test with the load force being applied at a constant rate of 1.5±0.5 mm/min. The metal-ceramic samples are grade 2 and grade 5 titanium samples anodized for 0, 1, 3, 5, 15, and 30 min (n=10) in electrolyte of ethylene glycol, 0.2 wt. % NH_4F, and 4 wt. % DI water at 60V.

The coefficient k [mm^{-2}] is a function of the thickness and Young's modulus value of the individual samples. The Young's modulus (E_M [GPa]) of the samples was calculated using data from the stress-strain graph from the TestWorks software linked to the universal testing machine with the following equation:

$$E_M = \frac{\sigma}{\varepsilon} \quad \text{.....Eqn. 2.2}$$

Stress is denoted by σ [GPa] and strain is denoted by ε.

Independent student t-tests revealed no significant increase in debonding strength by any anodized groups over the non-anodized metal-ceramic controls. Contrary to the hypothesis, the mean debonding strength of several anodized metal-ceramic groups was significantly lower than the non-anodized metal-ceramic controls: grade 2 metal-ceramic samples anodized for 1 and 15 min (p=0.001 and p=0.012, respectively) and grade 5 metal-ceramic samples anodized for 1 min (p=0.009). All the other samples showed no significant

increase or decrease in τ_b when compared to the corresponding control samples of the same grade ($p>0.05$).

From the F_{fail} and τ_b values as well as the student t-test results, it is apparent that the anodization of titanium did not significantly increase the bonding between titanium and porcelain. In certain cases, the anodization lowered the bonding between the titanium and porcelain. The images of the sample surfaces after debonding in figs. 2.15 and 2.16 help assess why the TNTs did not lead to stronger bonding between the titanium and porcelain. Figs. 2.15(a, c, e, and g) and 2.16(a, c, e, and g) show the anodized grade 2 and grade 5 titanium surfaces before porcelain application, while figs. 2.15(b, d, f, and h) and 2.16(b, d, f, and h) show the anodized grade 2 and grade 5 titanium surfaces after they were debonded from porcelain via the three point bending test. Figs. 2.15(a, c, e, and g) and 2.16(a, c, e, and g) all show the open tops of the TNTs on the anodized titanium surfaces. This was verified as being titanium dioxide using EDS analysis. Figs. 2.15(b, d, f, and h) and 2.16(b, d, f, and h) do not show these open tops of the TNTs. The flat and smooth portions on figs. 2.15(b, d, f, and h) and 2.16(b, d, f, and h) are porcelain that has adhered to the titanium during the debonding process. This was verified as being porcelain using EDS analysis. Horizontal TNTs with their sides broken are visible in figs. 2.15(b, d, f, and h). Also in these figures, deformed TNTs are visible on the surface. Figs. 2.16(b, d, f, and h) show TNTs that are distorted as well.

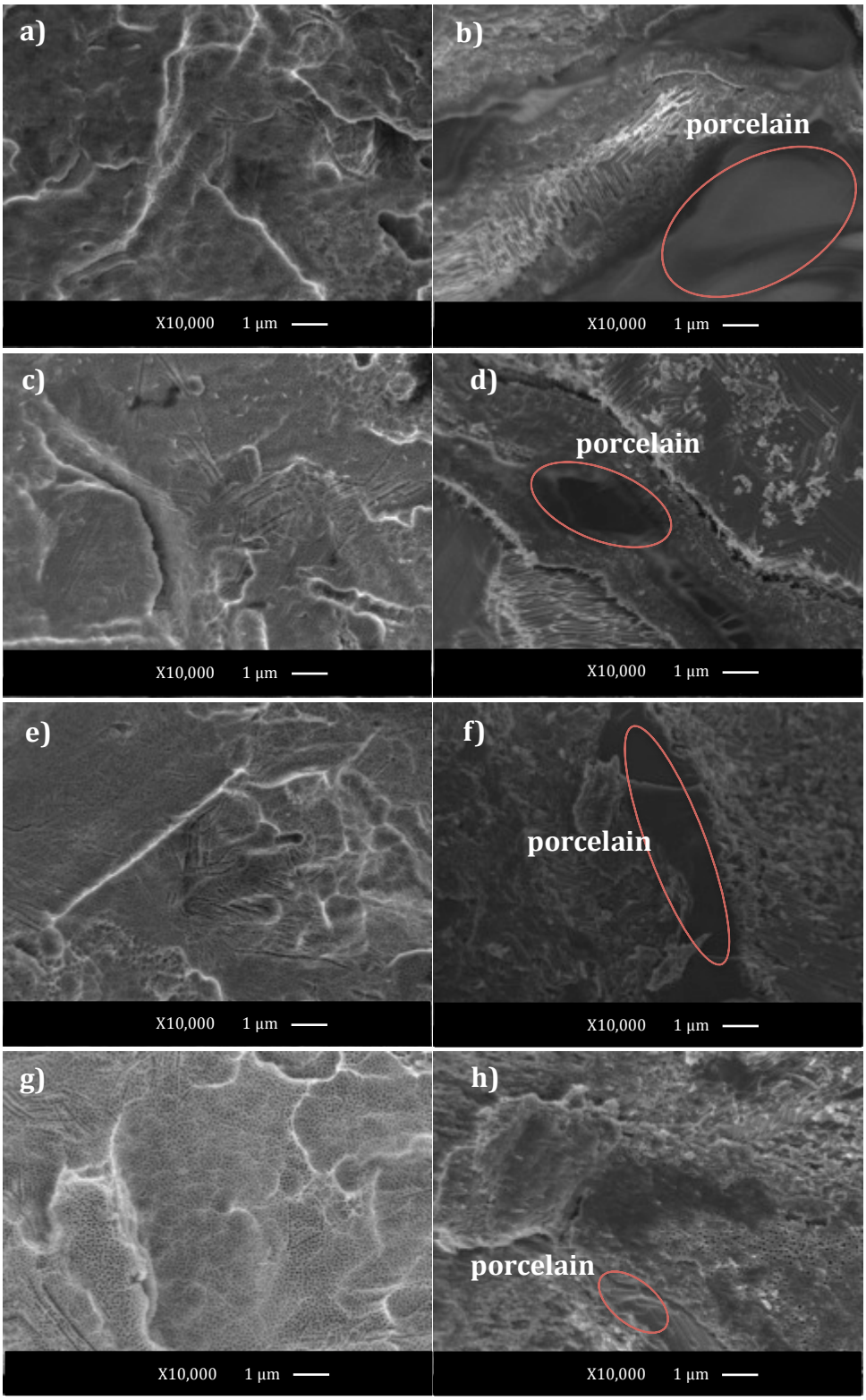

Figure 2.15 Grade 2 titanium samples that were anodized in an electrolyte of ethylene glycol, 0.2 wt. % NH_4F, and 4 wt. % DI water at 60V for 1, 5, 15, and 30 min. These samples were subsequently stacked with porcelain and fired with the schedule listed in Table 2, and subjected to the 3 point bending test. a) 10X FESEM image of grade 2 titanium sample anodized for 1 min; b) 10X FESEM image of 1 min anodized grade 2 sample after it was debonded from the porcelain post-3 point bending test; c) 10X FESEM image of grade 2 titanium sample anodized for 5 min; d) 10X FESEM image of 5 min

anodized grade 2 sample after it was debonded from the porcelain post-3 point bending test; e) 10X FESEM image of grade 2 titanium sample anodized for 15 min; f) 10X FESEM image of 15 min anodized grade 2 sample after it was debonded from the porcelain post-3 point bending test; g) 10X FESEM image of grade 2 titanium sample anodized for 30 min; h) 10X FESEM image of 30 min anodized grade 2 sample after it was debonded from the porcelain post-3 point bending test.

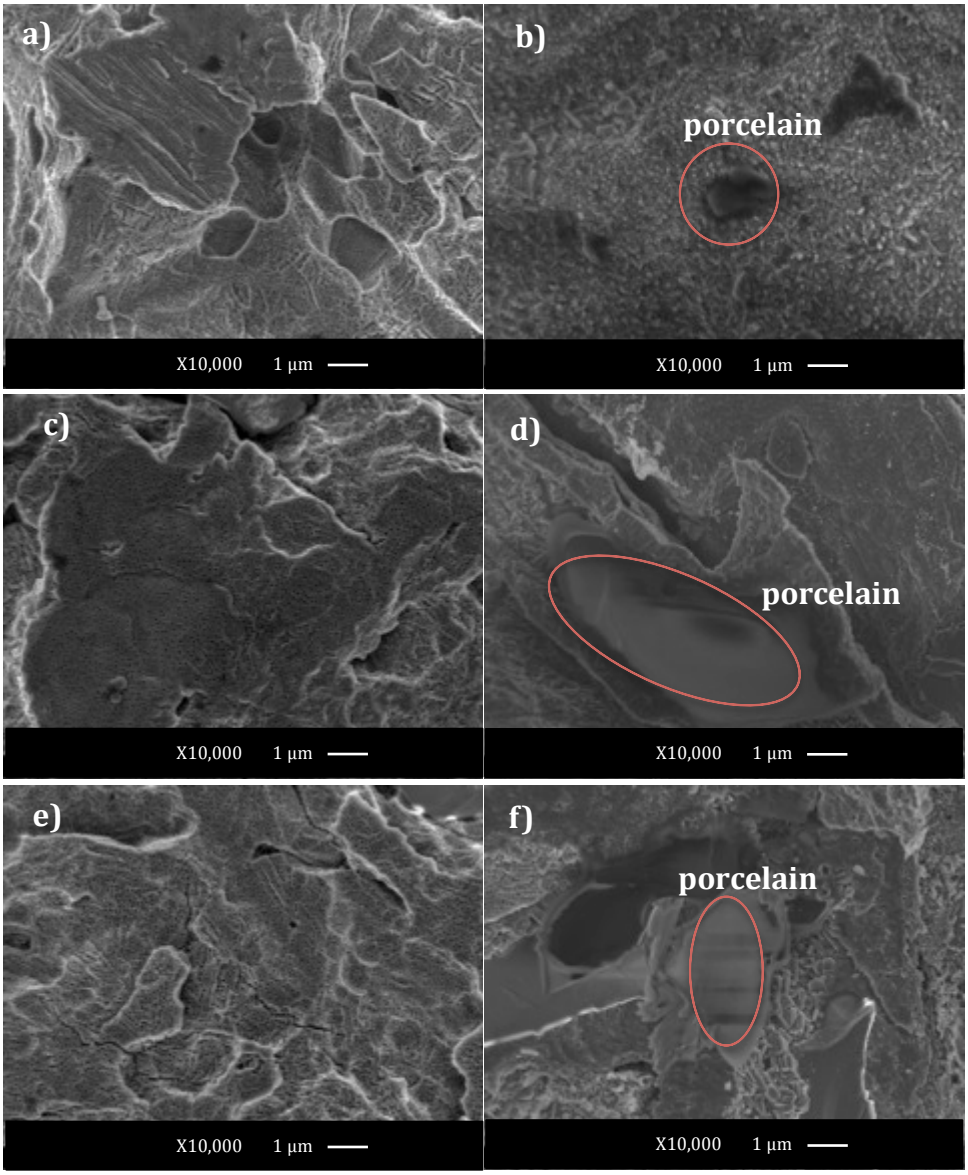

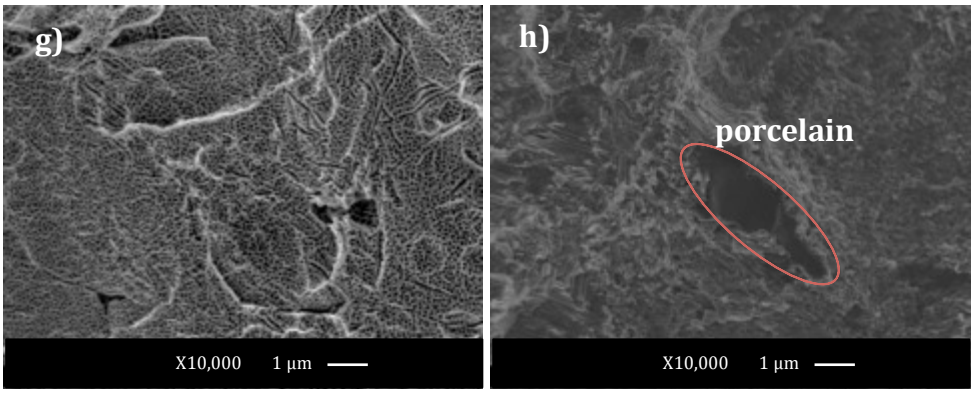

Figure 2.16 Grade 5 titanium samples that were anodized in an electrolyte of ethylene glycol, 0.2 wt. % NH_4F, and 4 wt. % DI water at 60V for 1, 5, 15, and 30 min. These samples were subsequently stacked with porcelain and fired with the schedule listed in Table 2, and subjected to the 3 point bending test. a) 10X FESEM image of grade 5 titanium sample anodized for 1 min; b) 10X FESEM image of 1 min anodized grade 5 sample after it was debonded from the porcelain post-3 point bending test; c) 10X FESEM image of grade 5 titanium sample anodized for 5 min; d) 10X FESEM image of 5 min anodized grade 5 sample after it was debonded from the porcelain post-3 point bending test; e) 10X FESEM image of grade 5 titanium sample anodized for 15 min; f) 10X FESEM image of 15 min anodized grade 5 sample after it was debonded from the porcelain post-3 point bending test; g) 10X FESEM image of grade 5 titanium sample anodized for 30 min; h) 10X FESEM image of 30 min anodized grade 5 sample after it was debonded from the porcelain post-3 point bending test.

TNTs are stable up to ~550°C (Roy et al., 2011) (Regonini et al., 2013). TNTs are reported to collapse above this temperature (Regonini, Jaroenworaluck, Stevens, & Bowen, 2010) (Regonini et al., 2013) (Cai, Paulose, Varghese, & Grimes, 2005). Thus, TNTs could have collapsed on the titanium samples during the porcelain firing process due to the exposure to high temperatures (~800°C) in the dental furnace. To test this, grade 2 and grade 5 titanium samples were prepared and subsequently anodized for 5 min using the preparation and anodization protocols mentioned in the Materials and Methods section. These samples were subjected to the firing conditions detailed in table 2.2. This course of action was taken to discovery how the TNTs reacted to the high heat of the dental furnace. The surfaces of the titanium samples were imaged using FESEM and are shown in figs. 2.17(a and c). These images reveal that the TNTs on both grades of titanium are disfigured and collapsed. There is a small amount of open tube tops visible on the surfaces, if any.

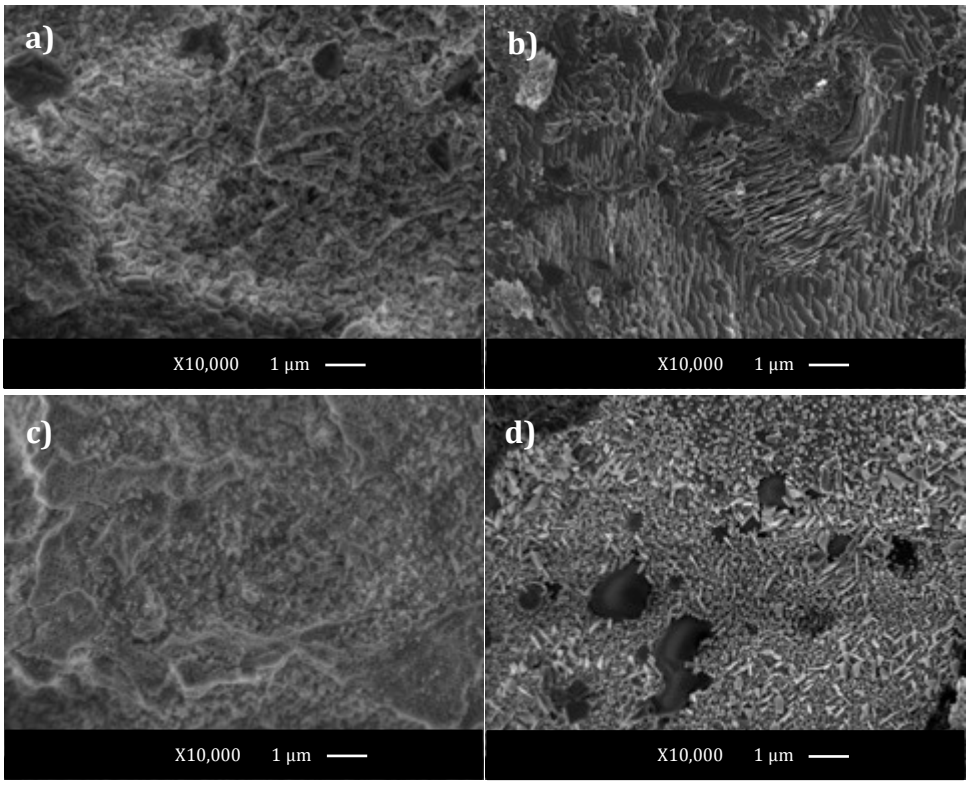

Figure 2.17 Grade 2 and grade 5 titanium samples were sandblasted, acid-etched, and anodized for 5 min in an electrolyte made of ethylene glycol, 0.2 wt. % NH_4F, and 4 wt. % DI water at 60V. These samples were subjected to the firing conditions detailed in table 2. a) 10X FESEM image of TNTs grown on grade 2 titanium after they were exposed to firing conditions in the dental furnace; b) 10X FESEM image of TNTs grown on grade 2 titanium after they were stacked with porcelain and exposed to firing conditions in the dental furnace, and had the porcelain manually removed from them (not via the 3 point bending test); c) 10X FESEM image of TNTs grown on grade 5 titanium after they were exposed to firing conditions in the dental furnace; d) 10X FESEM image of TNTs grown on grade 5 titanium after they were stacked with porcelain and exposed to firing conditions in the dental furnace, and had the porcelain manually removed from them.

Another cause of the TNTs' collapse could have been due to being crushed during the 3 point bending test step. The TNTs could have been protected from collapsing in the dental furnace by the porcelain applied on top. In order to test this, porcelain was applied onto grade 2 and grade 5 titanium samples which had been anodized for 5 min. These samples were placed in the dental furnace and fired. Then, the porcelain was removed from the titanium manually, not using the 3 point bending test. If the TNTs on these titanium surfaces had been protected by the porcelain by the porcelain melting into the TNTs or shielding the TNTs from the high heat of the dental furnace, or any other mechanism, then they would have remained upright. Then TNTs wouldn't have been crushed by the 3 point

bending test. From figs. 2.17(b and d), it is clear that TNTs didn't remain upright; once again, the open tube tops are not present. The TNTs in the images are disfigured. Therefore, the TNTs collapsed due to the high heat of the furnace, not during the 3 point bending step. The disruption in TNT structure could have lead to the low bonding between the anodized titanium samples and dental porcelain.

The anodized metal-ceramic samples with the longer nanotube lengths (grade 2 and grade 5 samples anodized for 1, 15, and 30 min) had a lower attachment to the porcelain compared to the samples with the short nanotube lengths (grade 2 and grade 5 samples anodized for 5 min). This can be seen in fig. 2.13. This qualitative trend could be due to the creation of voids between porcelain and titanium as a result of nanotubes collapsing in the dental furnace. When the longer nanotubes collapse, there are likely more voids created at the metal-ceramic interface. This could have led to the poorer attachment of samples with longer nanotubes to the porcelain.

The ANOVA analysis of the results revealed a significant increase in debonding strength of the grade 5 metal-ceramic samples over that of grade 2 metal-ceramic samples; the p-value of this was 0.028. Grade 2 titanium is more ductile than grade 5 titanium (Noort, 1987) and thus grade 2 titanium's susceptibility to bending may have led to its lower debonding strength. Other studies which subjected both grade 2 and grade 5 titanium samples to identical surface treatments and subsequent 3-point bending tests had similar results: grade 5 titanium had a higher debonding strength compared to grade 2 titanium (Bieniaś, Surowska, Stoch, Matraszek, & Walczak, 2009) (Suansuwan & Swain, 2003).

2.3.3 Analysis of break between titanium and porcelain

Porcelain was visible on each FESEM image taken of the grade 2 and grade 5 un-anodized and anodized titanium sides after the metal-ceramic samples had been subjected to the 3-point bending test (figs. 2.18, 2.20, 2.22, 2.24, and 2.26). This was verified as being porcelain by using EDS analysis.

Titanium dioxide was visible on the FESEM images taken of the porcelain sides that were connected to the un-anodized titanium samples (fig. 2.19). This was verified as being titanium dioxide by using EDS analysis. Figs. 2.18 and 2.19 indicate that the break for the un-anodized metal-ceramic samples occurred in a jagged fashion.

The broken tops of TNTs were visible on the FESEM images taken of the porcelain connected to the anodized titanium samples (figs. 2.21, 2.23, 2.25 and 2.27). These were verified as being made of titanium dioxide by using EDS analysis. This indicates that the TNTs were pulled apart in the 3-point bending process; their structure was not strong enough to stay intact. In conclusion, for every metal-ceramic sample, the break during the 3-point bending test appears to have occurred in a jagged fashion. Thus, the break was apparently both a substrate failure and cohesive failure. Substrate failure refers to the dental porcelain breaking off and sticking to the corresponding titanium samples. Cohesive failure refers to when the cohesive strength of the particles within the adhesive are not as strong as the adhesive's bond to the substrate. In this study the adhesive refers to the TNTs for the anodized samples and the titanium dioxide layer for the roughened samples. The substrates that the adhesive is bound to are the titanium metal and dental porcelain.

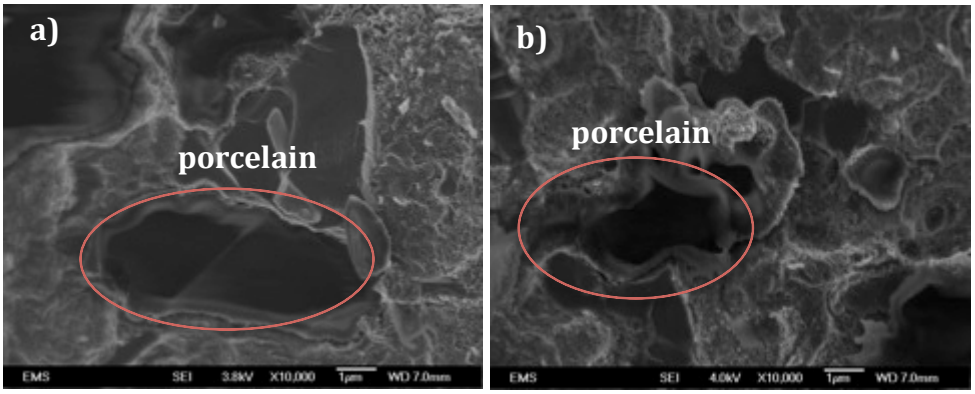

Figure 2.18 10X FESEM images of a) unanodized grade 2 titanium and b) unanodized grade 5 titanium that were attached to porcelain.

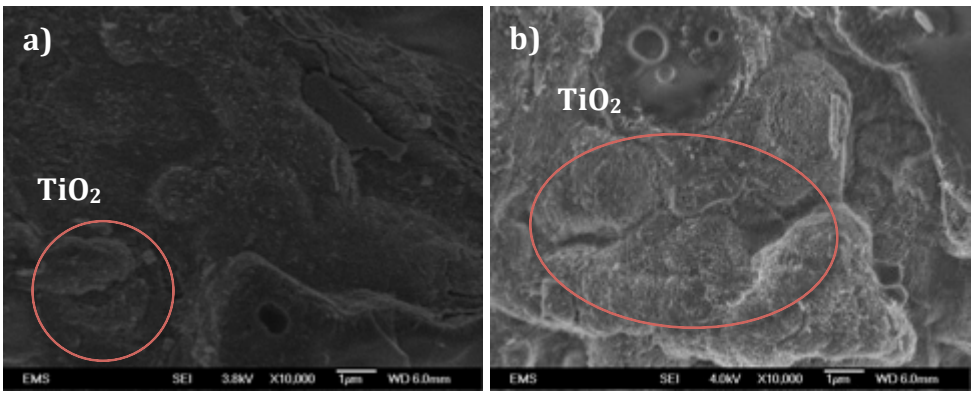

Figure 2.19 10X FESEM images of a) porcelain that was attached to roughened grade 2 metal and b) porcelain that was attached to roughened grade 5 metal.

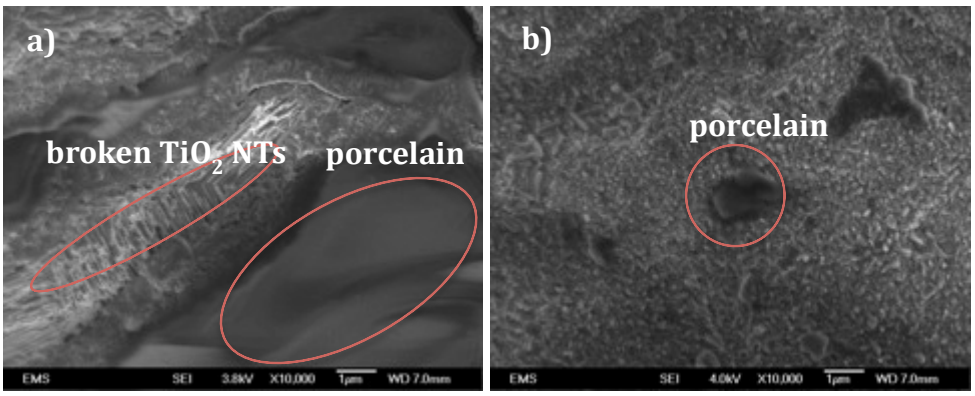

Figure 2.20 10X FESEM images of a) 1 min anodized grade 2 titanium and b) 1 min anodized grade 5 titanium that were attached to porcelain.

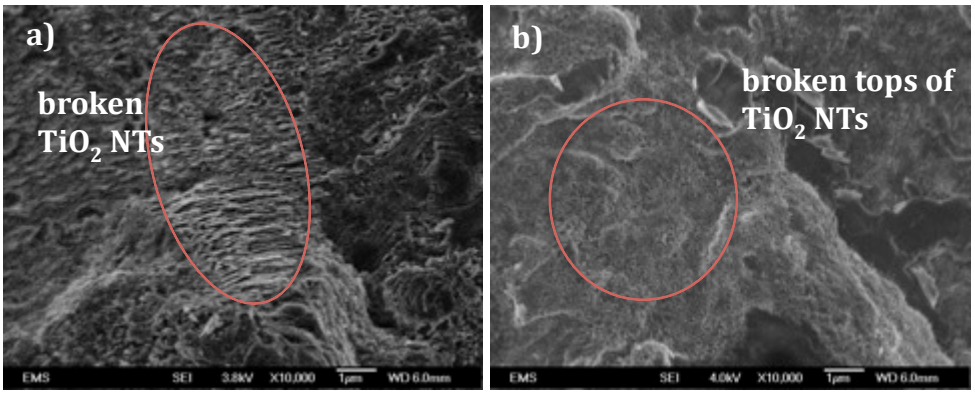

Figure 2.21 10X FESEM images of a) porcelain that was attached to 1 min anodized grade 2 metal and b) porcelain that was attached to 1 min anodized grade 5 metal.

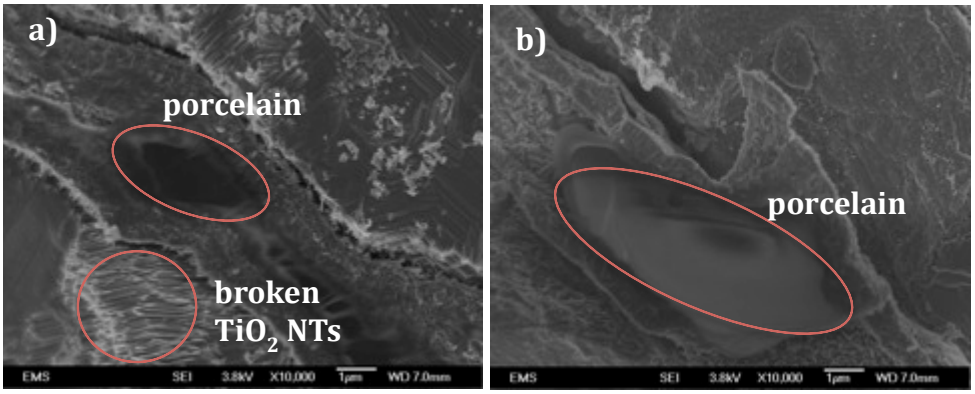

Figure 2.22 10X FESEM images of a) 5 min anodized grade 2 titanium and b) 5 min anodized grade 5 titanium that were attached to porcelain.

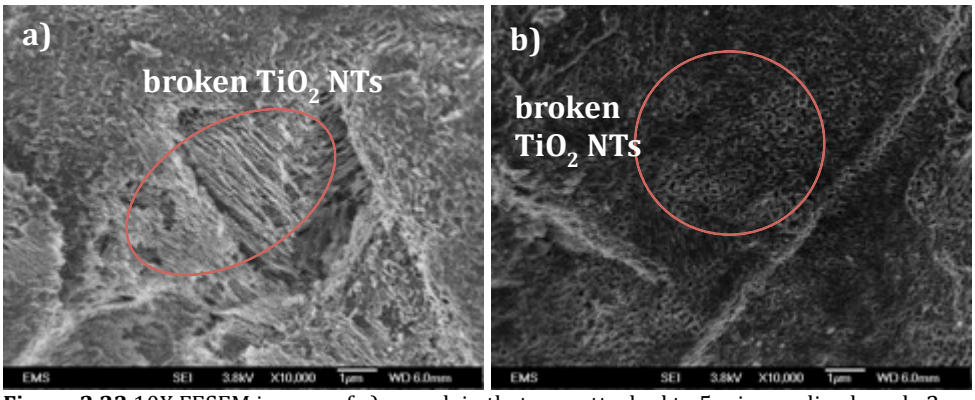

Figure 2.23 10X FESEM images of a) porcelain that was attached to 5 min anodized grade 2 metal and b) porcelain that was attached to 5 min anodized grade 5 metal.

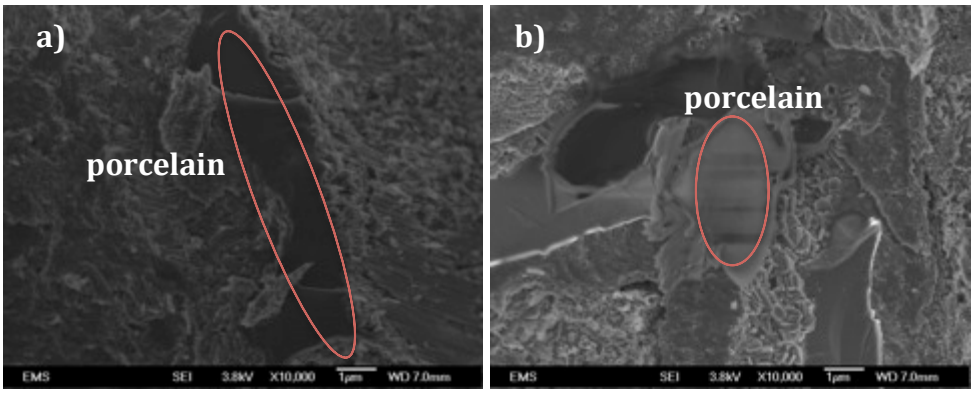

Figure 2.24 10X FESEM images of a) 15 min anodized grade 2 and b) 15 min anodized grade 5 titanium that were attached to porcelain.

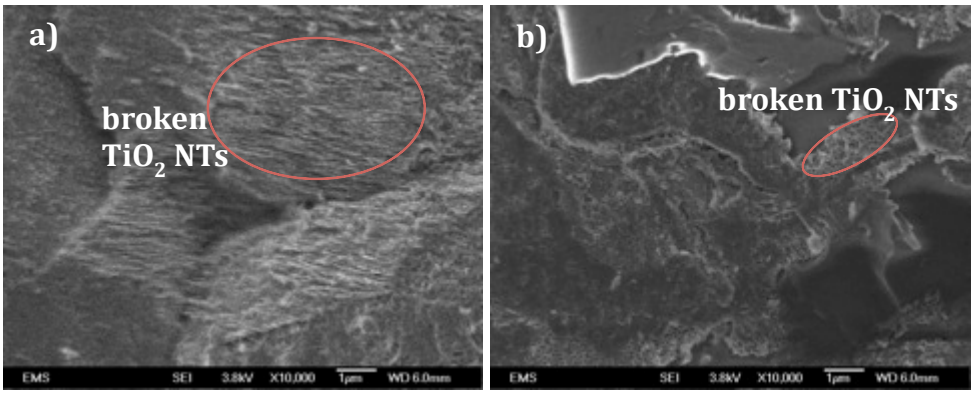

Figure 2.25 10X FESEM images of a) porcelain that was attached to 15 min anodized grade 2 metal and b) porcelain that was attached to 15 min anodized grade 5 metal.

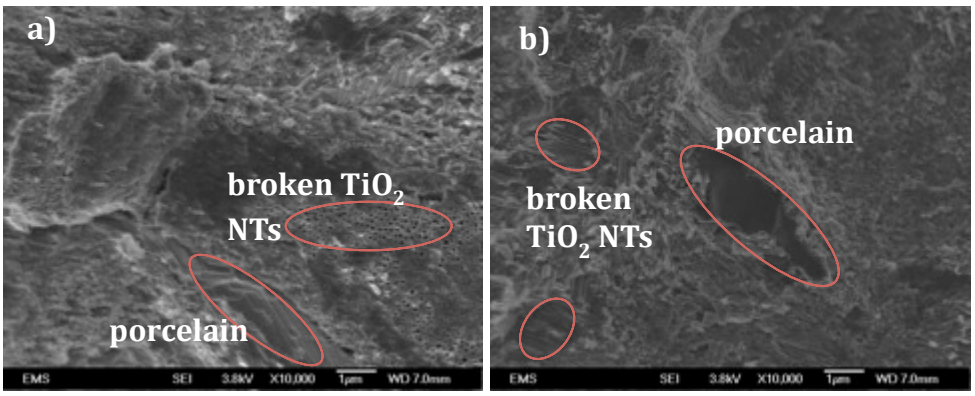

Figure 2.26 10X FESEM images of a) 30 min anodized grade 2 titanium and b) 30 min anodized grade 5 titanium that were attached to porcelain.

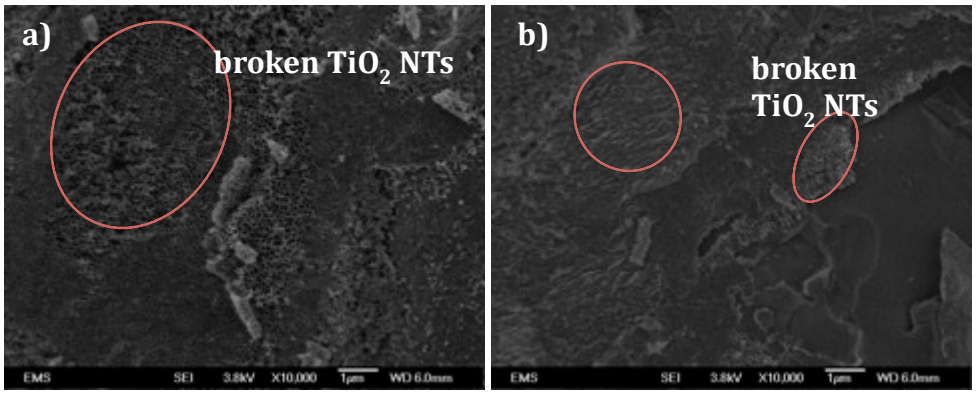

Figure 2.27 10X FESEM images of a) porcelain that was attached to 30 min anodized grade 2 metal and b) porcelain that was attached to 30 min anodized grade 5 metal.

2.4 Conclusion

The investigation of electrochemical anodization surface treatment on grade 2 and grade 5 titanium showed that growing TNTs on the surface of the metals did not significantly increase the adhesion between the TNTs and ceramic. In fact, student t-test results showed that the mean debonding strength of grade 2 metal-ceramic samples anodized for 1 and 15 min and grade 5 metal-ceramic samples anodized for 1 min was significantly lower ($p<0.05$) than the non-anodized controls. TNTs collapse when exposed to the high temperatures in the dental furnace. Thus, it is not recommended that TNTs be used in PFM applications. These findings suggest that there is a need for further research on developing a different coating that can withstand the high temperatures in the dental furnace, lead to successful wetting of porcelain on the metal surface, and successfully achieve stronger bonding between the titanium and dental porcelain during the firing process.

Chapter 3

Future work: Proposal for Coating to Act as a Barrier for Diffusion of Oxygen

3.1 Introduction

3.1.1 Background and Previous Coatings

Since the TNTs grown between the dental porcelain and titanium did not significantly increase their bonding, a different method of increasing the bonding is proposed. As mentioned in the introduction section, titanium and its alloys readily react with oxygen during the porcelain firing process, which leads to excessive oxidation. During the ~800°C temperature exposure of the porcelain firing process, the reactive titanium tends to form a brittle oxide layer. This oxide layer does not bond well to the dental porcelain above it.

There is a need for a protective coating on the titanium to avoid the nonadherent titanium oxide growth. In previous experiments, the coatings were deposited on titanium using mainly physical vapor deposition (PVD) methods (Table 3.1).

Table 3.1 Coating methods used in in previous studies.

Coating Method	**Coating Material(s)**	**Thickness(es) of Coating(s)**	**Reference(s)**
Arc ion plating system	TiN	5,000 nm	(S. Park et al., 2009)
Sputter coating	Au	150 nm to 2,000 nm	(Khung & Suansuwan, 2013), (S. Park et al., 2009)
Cold thermal spraying	ZrO_2-CaO, Ni-Al-Mo+ ZrO_2-CaO	100,000 nm	(Marcelli et al., 2014)
Plasma-immersion implantation and deposition	Si_3N_4	1,000 nm	(Wang et al., 1999)
Radio frequency reactive magnetron sputtering	ZrSiN	1,000 nm	(H. Zhang, Guo, Song, Wang, & Xu, 2007)

Chemical vapor deposition (CVD) methods have advantages over PVD methods. The coatings produced by CVD are conformal. The insides and undersides of surfaces with macro-level and nano-level roughness can be completely covered with the same thickness of coating (J.-H. Park & Sudarshan, 2001). This is highly important for titanium that is to be put into environments where it is highly reactive. In contrast, PVD is a line of sight technique and has difficulty coating tortuous surface features.

3.1.2 Atomic Layer Deposition

Atomic layer deposition (ALD) is a CVD method of producing thin films. During this process, a mixture of gases flows over a heated substrate and causes a thin solid film to grow on the surface.

ALD is mainly a two step process. First, the substrate to be coated is exposed to the preliminary reactant in the ALD chamber. The reactant is then pumped away using an inert gas. A monolayer of this reactant adsorbs to the surface and remains there after chamber is evacuated. The forces holding the molecular species on the surface can be physical adsorption or chemisorption. A second reactant enters the ALD chamber and converts the first reactant to a layer of the desired solid material. This second reactant is also removed from the chamber. This process (fig. 3.1) is repeated to get a film of the desired thickness (Kääriäinen, Cameron, Kääriäinen, & Sherman, 2013). ALD is proposed to coat titanium used in PFMs with the aim of increasing the bonding between titanium and dental porcelain.

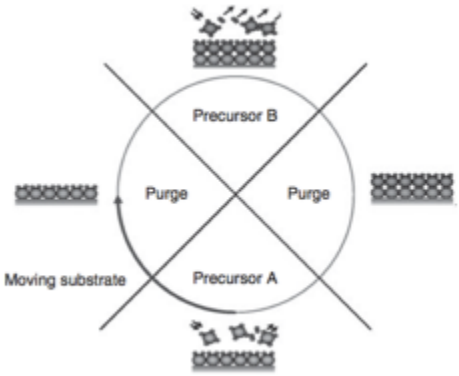

Figure 3.1 Schematic of ALD cycle (Kääriäinen et al., 2013).

3.1.3 Proposed Chemical Coating

The coating on titanium can either form an adherent oxide film that sticks to both titanium and the dental porcelain or it can be inert. Inert, noble metals are often expensive and difficult to deposit using ALD. Therefore, it is cost-effective and practical to develop a coating that can form an adherent oxide film. The free energy change for the formation of the metal oxide of the coating must be more negative than that of titanium dioxide. That way, during the firing process the chemicals in the coating will more readily form oxide than titanium (Sung & Kim, 2005).

Ellingham diagrams are plots of ΔG versus temperature. They can be used to pick out metal oxides with lower free energies of formation compared to that of titanium dioxide at temperatures reached in the dental furnace (the highest will be ~800°C, 1074 K) ("The Interactive Ellighan Diagram"). Zirconium dioxide (ZrO_2) and hafnium dioxide (HfO_2) fit the criteria in the designated temperature range (fig. 3.2).

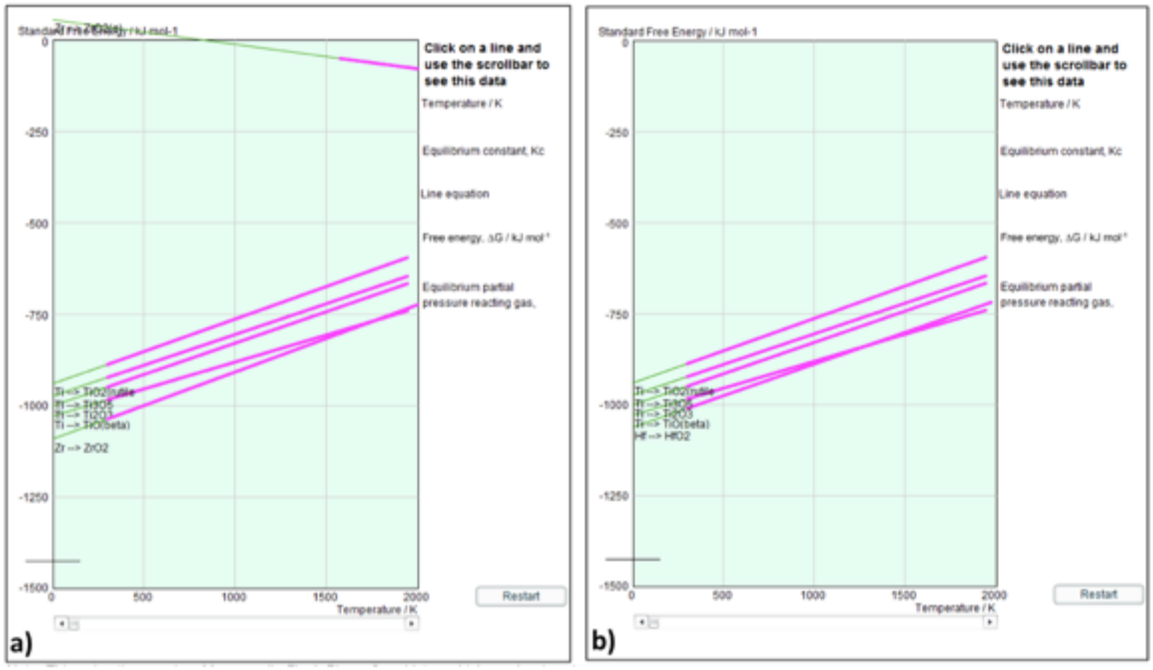

Figure 3.2 Ellingham diagram comparing a) Gibbs free energies of titanium dioxides and ZrO_2 as well as b) Gibbs free energies of titanium dioxides and HfO_2 ("The Interactive Ellighan Diagram").

The difference in the free energy of formation of ZrO_2 and TiO_2 is higher than that of HfO_2 and TiO_2. ZrO_2 has a monoclinic crystal structure at room temperature and transitions to tetragonal and cubic structure at higher temperatures. The volume expansion from the transition to tetragonal and cubic phases causes high stress, which result in ZrO_2 cracking open upon cooling from higher temperatures (Basu, 2005). Dopants, such as yttria (Y_2O_3), are used to stabilize the ZrO_2 at high temperatures in the tetragonal and cubic phase. The Gibbs free energy of Y_2O_3 is also less than that of titanium oxides in the temperature range as shown in fig. 3.2.

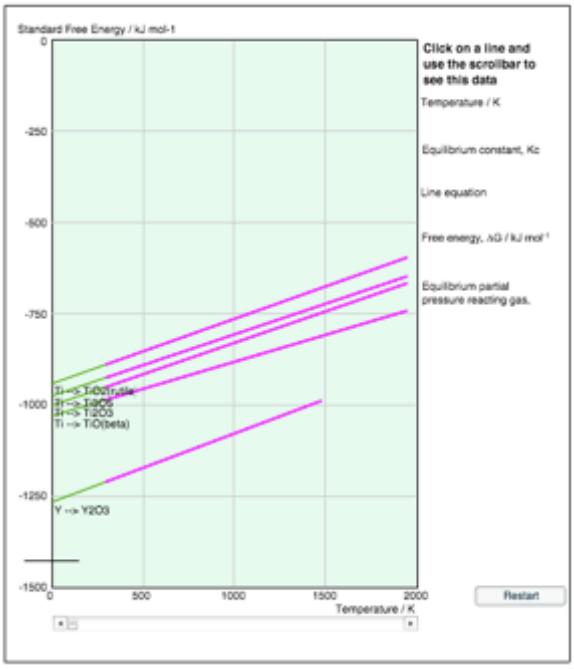

Figure 3.3 Ellingham diagram comparing a) Gibbs free energies of titanium dioxides and Y_2O_3 ("The Interactive Ellighan Diagram").

ALD deposition of yttria-stabilized zirconia (YSZ) has been done before by (Xu, Selvaraj, Jursich, Feinerman, & Takoudis, 2013). In the investigation, ALD was done at 270^0C. The precursor used for yttrium was tris(isopropyl-cyclopentadienyl)yttrium ($Y(iPrCp)_3$) and the precursor used for zirconium was tris(demethylamino)cyclopentadienyl zirconuim ($ZrCp(NMe_2)_3$). Ozone was used as the oxidant.

Thus if ALD is used to deposit YSZ on top of titanium, the yttria content will need to be optimized so that its CTE matches that of the titanium (9.4×10^{-6}/°C) (Yilmaz & Dinçer, 1999). It has been shown that the CTE of YSZ decreases as the content of Y_2O_3 increases (fig. 3.4) (Hayashi et al., 2005).

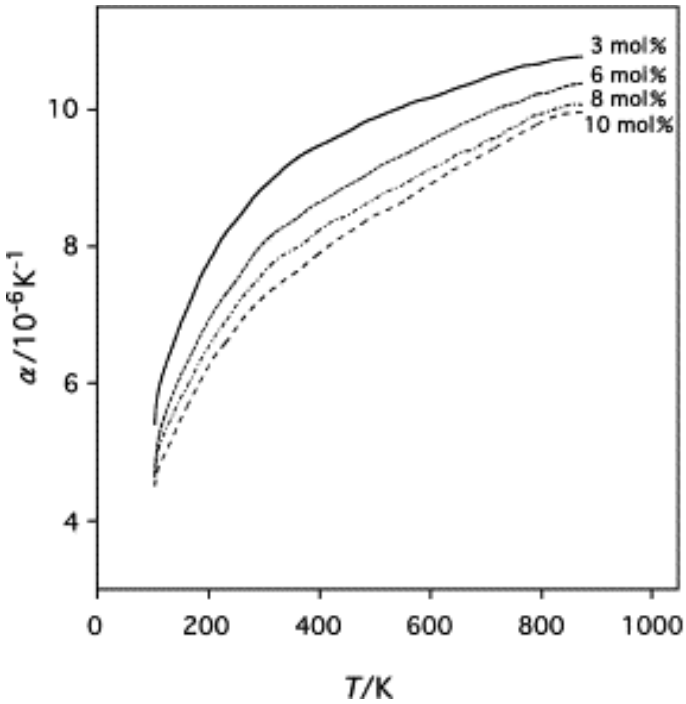

Figure 3.4 Thermal expansion coefficient of YSZ with various Y2O3 content measured by a dilatometer (Hayashi et al., 2005).

3.2 Experimental Procedure

ISO standards will be used when preparing groups of grade 2 and grade 5 samples again. The mechanical interlocking of titanium and porcelain will be promoted through sandblasting and acid-etching titanium samples, using similar protocols as listed in Section 2.2.2.

The samples will then be coated with yttria-stabilized zirconia via ALD. The thickness of the coating will be measured using spectral ellipsometry. The composition of the YSZ coating will be determined using X-ray photoelectron spectroscopy (XPS).

Low-fusing porcelain will be added and fired on the coated titanium samples as detailed in Section 2.2.5. The samples will be subjected to the three-point bending test to evaluate the bonding strength between titanium and dental porcelain using the apparatus and parameters listed in 2.2.6. The type of failure that the debonded titanium and porcelain samples underwent will be evaluated by FESEM imaging, as outlined in Section 2.2.6.

Chapter 4

Clinical Scope

4.1 Relevance and Application

This study demonstrated the impracticality on relying on purely mechanical retention for increasing the bonding between titanium and dental porcelain in PFMs. A two-pronged approach of both mechanical interlocking and creation of a chemical barrier to oxidation will lead to the strongest PFMs. When such an intermediate between titanium and porcelain is achieved, it has direct clinical relevance. The titanium copings can be prepared with the chemical coating and directly cemented into the dental patients' mouths. The ultimate aim of this work is to increase the longevity of PFMs so patients do not have to go through the painful and expensive process of replacing them.

References

1. Adachi, M., Mackert, J. R., Parry, E. E., & Fairhurst, C. W. (1990). Oxide Adherence and Porcelain Bonding to Titanium and Ti-6A1-4V Alloy. *Journal of Dental Research*, *69*(6), 1230–1235.
2. Akova, T., Ucar, Y., Tukay, A., Balkaya, M. C., & Brantley, W. A. (2008). Comparison of the bond strength of laser-sintered and cast base metal dental alloys to porcelain. *Dental Materials*, *24*(10), 1400–1404.
3. Asthana, A., Shofuhkar, T., Gao, Q., Heiden, P., Friedrich, C., & Yassar, R. (2010). A Study on the Modulation of the Electrical Transport by Mechanical Straining of Individual Titanium di Oxide Nanotube. *Microscopy and Microanalysis*, *16*(Supplement S2), 1386–1387.
4. Basu, B. (2005). Toughening of yttria-stabilised tetragonal zirconia ceramics. *International Materials Reviews*, *50*(4), 239–256.
5. Bergmann, C. P., & Stumpf, A. (2013). *Dental Ceramics: Microstructure, Properties and Degradation*. Springer Science & Business Media.
6. Bieniaś, J., Surowska, B., Stoch, A., Matraszek, H., & Walczak, M. (2009). The influence of SiO2 and SiO2–TiO2 intermediate coatings on bond strength of titanium and Ti6Al4V alloy to dental porcelain. *Dental Materials*, *25*(9),
7. Bjursten, L. M., Rasmusson, L., Oh, S., Smith, G. C., Brammer, K. S., & Jin, S. (2010). Titanium dioxide nanotubes enhance bone bonding in vivo. *Journal of Biomedical Materials Research Part A*, *92A*(3), 1218–1224.
8. Cai, Q., Paulose, M., Varghese, O. K., & Grimes, C. A. (2005). The Effect of Electrolyte Composition on the Fabrication of Self-Organized Titanium Oxide Nanotube Arrays by Anodic Oxidation. *Journal of Materials Research*, *20*(01), 230–236.
9. Darvell, B. W. (2009). *Materials Science for Dentistry* (9th ed.).
10. de Melo, R. M., Travassos, A. C., & Neisser, M. P. (2005). Shear bond strengths of a ceramic system to alternative metal alloys. *The Journal of Prosthetic Dentistry*, *93*(1), 64–69.
11. Diserens, M., Patscheider, J., & Lévy, F. (1999). Mechanical properties and oxidation resistance of nanocomposite TiN–SiNx physical-vapor-deposited thin films. *Surface and Coatings Technology*, *120–121*, 158–165.
12. Dong Hwan Shin, T. S. (2011). Wettability changes of TiO2 nanotube surfaces. *Nanotechnology*, *22*(31), 315704.
13. Fu, J., Wang, Y.-K., Yang, M. T., Desai, R. A., Yu, X., Liu, Z., & Chen, C. S. (2010). Mechanical regulation of cell function with geometrically modulated elastomeric substrates. *Nature Methods*, *7*(9), 733–736.
14. Guo, L., Tian, J., Wu, J., Li, B., Zhu, Y., Xu, C., & Qiang, Y. (2013). Effect of nano-porous film on the bonding strength of titanium–porcelain. *Materials Letters*, *109*, 140–142.
15. Hamlekhan, A., Butt, A., Patel, S., Royhman, D., Takoudis, C., Sukotjo, C., … Shokuhfar, T. (2014). Fabrication of Anti-Aging TiO2 Nanotubes on Biomedical Ti Alloys. *PLoS ONE*, *9*(5), e96213.
16. Hayashi, H., Saitou, T., Maruyama, N., Inaba, H., Kawamura, K., & Mori, M. (2005). Thermal expansion coefficient of yttria stabilized zirconia for various yttria contents. *Solid State Ionics*, *176*(5–6), 613–619.
17. Introduction to Energy Dispersive X-ray Spectrometry (EDS). (2014). UC RIverside.

18. Kääriäinen, T., Cameron, D., Kääriäinen, M.-L., & Sherman, A. (2013). *Atomic Layer Deposition: Principles, Characteristics, and Nanotechnology Applications* (2nd ed.). Scrivener Publishing LLC.
19. Khung, R., & Suansuwan, N. S. (2013). Effect of gold sputtering on the adhesion of porcelain to cast and machined titanium. *The Journal of Prosthetic Dentistry*, *110*(1), 41–46.
20. Kim, D., Ghicov, A., & Schmuki, P. (2008). TiO2 Nanotube arrays: Elimination of disordered top layers ("nanograss") for improved photoconversion efficiency in dye-sensitized solar cells. *Electrochemistry Communications*, *10*(12), 1835–1838.
21. Lei, B.-X., Luo, Q.-P., Sun, Z.-F., Kuang, D.-B., & Su, C.-Y. (2013). Fabrication of partially crystalline TiO2 nanotube arrays using 1, 2-propanediol electrolytes and application in dye-sensitized solar cells. *Advanced Powder Technology*, *24*(1), 175–182.
22. Lim, H.-P., Kim, J.-H., Lee, K.-M., & Park, S.-W. (2011). Fracture load of titanium crowns coated with gold or titanium nitride and bonded to low-fusing porcelain. *The Journal of Prosthetic Dentistry*, *105*(3), 164–170.
23. Litong Guo, Xiaochen Liu, Jiqiang Gao, Jianfeng Yang, Tianwen Guo, & Yabo Zhu. (2010). Effect of Surface Modifications on the Bonding Strength of Titanium-Porcelain. *Materials & Manufacturing Processes*, *25*(8), 710–717.
24. Marcelli, E., Costantino, M. L., Villa, T., Bagnoli, P., Zannoli, R., Corazza, I., & Cercenelli, L. (2014). Effect of intermediate ZrO2-CaO coatings deposited by cold thermal spraying on the titanium-porcelain bond in dental restorations. *The Journal of Prosthetic Dentistry*, *112*(5), 1201–1211.
25. Noort, R. V. (1987). Titanium: The implant material of today. *Journal of Materials Science*, *22*(11), 3801–3811.
26. O'Brien, W. J. (1997). *Dental materials and their selection*. Chicago: Quintessence Pub. Co.
27. Park, J.-H., & Sudarshan, T. S. (2001). *Chemical Vapor Deposition*. ASM International.
28. Park, S., Kim, Y., Lim, H., Oh, G., Kim, H., Ong, J. L., & Lee, K. (2009). Gold and titanium nitride coatings on cast and machined commercially pure titanium to improve titanium–porcelain adhesion. *Surface and Coatings Technology*, *203*(20–21), 3243–3249.
29. Patel, S. B., Hamlekhan, A., Royhman, D., Butt, A., Yuan, J., Shokuhfar, T., … Takoudis, C. G. (2014). Enhancing surface characteristics of Ti–6Al–4V for bio-implants using integrated anodization and thermal oxidation. *Journal of Materials Chemistry B*, *2*(23), 3597–3608.
30. Popat, K. C., Leoni, L., Grimes, C. A., & Desai, T. A. (2007). Influence of engineered titania nanotubular surfaces on bone cells. *Biomaterials*, *28*(21), 3188–3197.
31. Porcelain Fused to Metal « A-1 Dental Lab. (n.d.).
32. Powers, R. L. S. M. (Ed.). (2012). Chapter 11 - Restorative Materials—Ceramics. In *Craig's Restorative Dental Materials (Thirteenth Edition)* (pp. 253–275). Saint Louis: Mosby.
33. Rasmussen, S. T., Ngaji-Okumu, W., Boenke, K., & O'Brien, W. J. (1997). Optimum particle size distribution for reduced sintering shrinkage of a dental porcelain. *Dental Materials*, *13*(1), 43–50.

34. Regonini, D., Bowen, C. R., Jaroenworaluck, A., & Stevens, R. (2013). A review of growth mechanism, structure and crystallinity of anodized TiO2 nanotubes. *Materials Science and Engineering: R: Reports*, *74*(12), 377–406.
35. Regonini, D., Jaroenworaluck, A., Stevens, R., & Bowen, C. r. (2010). Effect of heat treatment on the properties and structure of TiO2 nanotubes: phase composition and chemical composition. *Surface and Interface Analysis*, *42*(3), 139–144.
36. Roy, P., Berger, S., & Schmuki, P. (2011). TiO2 Nanotubes: Synthesis and Applications. *Angewandte Chemie International Edition*, *50*(13), 2904–2939.
37. Shillingburg, H. T., Jacobi, R., & Brackett, S. E. (1987). *Fundamentals of tooth preparations for cast metal and porcelain restorations*. Quintessence Publishing Company. Retrieved from
38. Shokuhfar, T., Sinha-Ray, S., Sukotjo, C., & Yarin, A. L. (2013). Intercalation of anti-inflammatory drug molecules within TiO2 nanotubes. *RSC Advances*, *3*(38), 17380.
39. Song, Y.-Y., Schmidt-Stein, F., Bauer, S., & Schmuki, P. (2009). Amphiphilic TiO2 Nanotube Arrays: An Actively Controllable Drug Delivery System. *Journal of the American Chemical Society*, *131*(12), 4230–4232.
40. Suansuwan, N., & Swain, M. V. (2003). Adhesion of porcelain to titanium and a titanium alloy. *Journal of Dentistry*, *31*(7), 509–518.
41. Sung, S.-Y., & Kim, Y.-J. (2005). Alpha-case formation mechanism on titanium investment castings. *Materials Science and Engineering: A*, *405*(1–2), 173–177.
42. University of Cambridge. (2015). *The Interactive Ellingham Diagram*.
43. Wagner, W. C., Asgar, K., Bigelow, W. C., & Flinn, R. A. (1993). Effect of interfacial variables on metal-porcelain bonding. *Journal of Biomedical Materials Research*, *27*(4), 531–537.
44. Wang, R. R., Welsch, G. E., & Monteiro, O. (1999). Silicon nitride coating on titanium to enable titanium–ceramic bonding. *Journal of Biomedical Materials Research*, *46*(2), 262–270.
45. Wyant, J. C. (2002). White Light Interferometry. In *Proceedings of SPIE* (Vol. 4737, p. 99).
46. Xu, R., Selvaraj, S. K., Jursich, G., Feinerman, A., & Takoudis, C. (2013). Nucleation Behavior-Morphology-Resistivity of Atomic Layer Deposited Pt on Atomic Layer Deposited Yttria-Stabilized Zirconia Films. *ECS Journal of Solid State Science and Technology*, *2*(11), P452–P456.
47. Yao, H., & Kimura, K. (2007). Field Emission Scanning Electron Microscopy for Structural Characterization of 3D Gold Nanoparticle Superlattices. *Modern Research and Educational Topics in Microscopy*.
48. Yilmaz, H., & Dinçer, C. (1999). Comparison of the bond compatibility of titanium and an NiCr alloy to dental porcelain1. *Journal of Dentistry*, *27*(3), 215–222.
49. Yin, H., Liu, H., & Shen, W. Z. (2010). The large diameter and fast growth of self-organized TiO2 nanotube arrays achieved via electrochemical anodization. *Nanotechnology*, *21*(3), 035601.
50. Yoriya, S., Kittimeteeworakul, W., & Punprasert, N. (2012). Effect of Anodization Parameters on Morphologies of TiO2 Nanotube Arrays and Their Surface Properties. *J. Chem. Chem. Eng*, *6*, 686–691.

51. Zhang, H., Guo, T. W., Song, Z. X., Wang, X. J., & Xu, K. W. (2007). The effect of ZrSiN diffusion barrier on the bonding strength of titanium porcelain. *Surface and Coatings Technology*, *201*(9–11), 5637–5640.
52. Zhang, T., Li, X., Wu, X., Shaozhou, W., Bai, X., Liu, S., … Zhang, Y. (2014). Characterization of monoclonal antibodies against duck hepatitis type 1 virus VP1 protein. *Journal of Virological Methods*, *208*(0), 166–170.
53. Zygo Corporation. (n.d.). Surface Texture Parameters.

Supplementary Figures

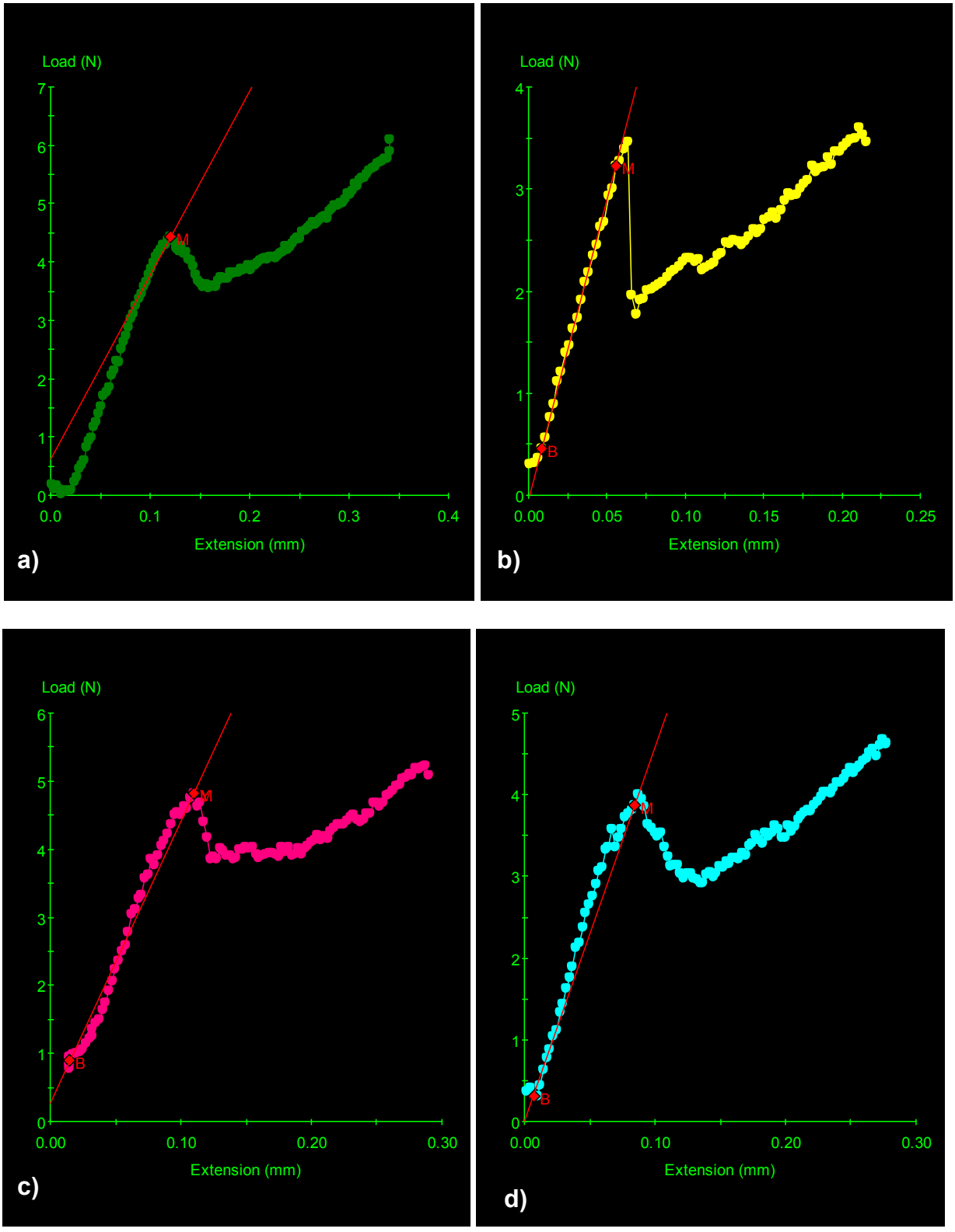

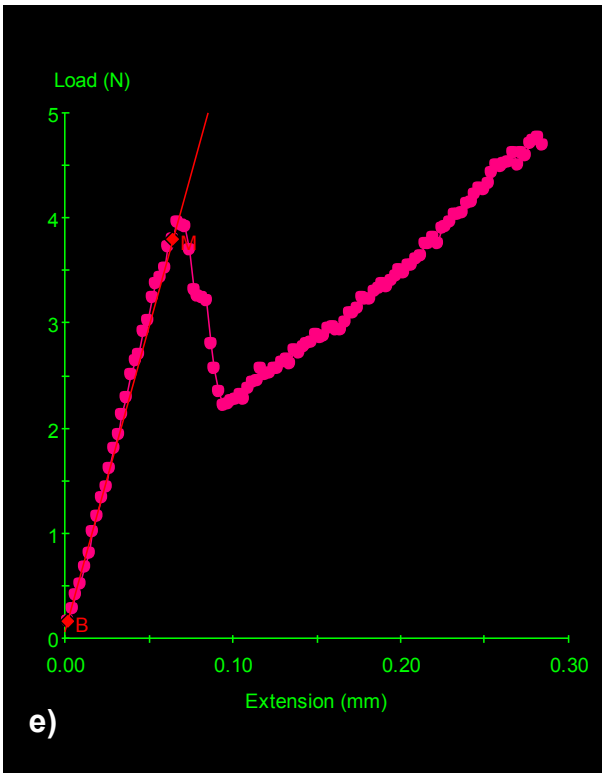

Supplementary figure 1 Load-displacement graphs for grade 2 titanium samples anodized for a) 0, b) 1, c) 5, d) 15, and e) 30 min.

VITA

NAME:	Himani Nadgauda
EDUCATION:	B.S., Chemical Engineering, Univeristy of California, Berkeley, Berkeley, California, 2013 M.S., Chemical Engineering, University of Illinois at Chicago, Chicago, Illinois, 2015
TEACHING EXPERIENCE:	Department of Chemical Engineering, University of Illinois at Chicago, Chicago, Illinois, 2013: Introductory Chemical Engineering course
PROFESSIONAL MEMBERSHIP:	Society of Women Engineers